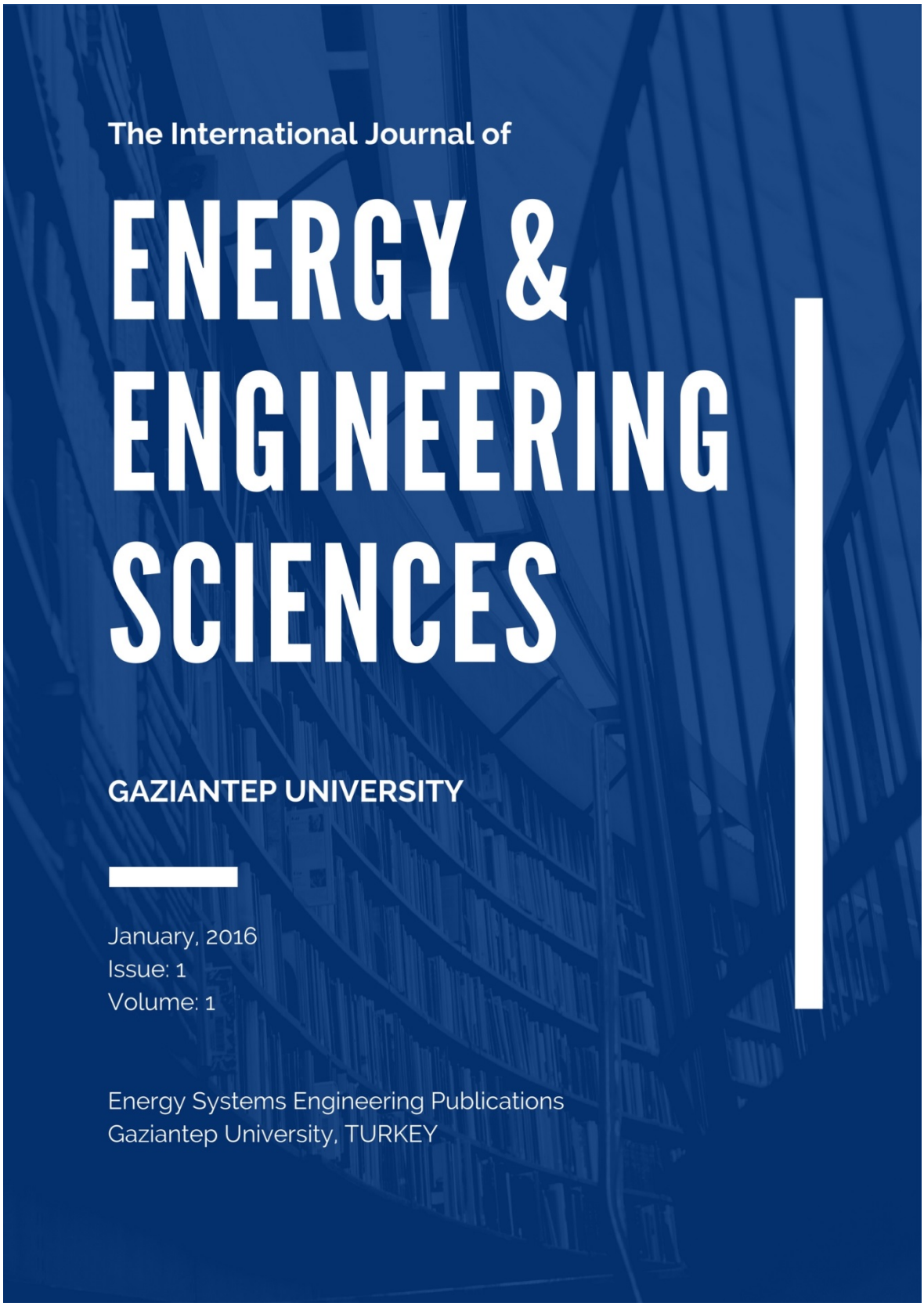

January, 2016
Issue: 1
Volume: 1

Energy Systems Engineering Publications
Gaziantep University, TURKEY

Editor In Chief Asst. Prof. Dr. Adem Atmaca
Co-Editor Asst. Prof. Dr. Nihat Atmaca

Gaziantep University Engineering Faculty
+90 342 360 12 00
+90 342 360 10 13
gaziantep.university.ijees@gmail.com
https://uemk-conferences.wixsite.com/ijees

Published by

Gaziantep university, Engineering Faculty, Energy Systems Engineering,
Üniversite Bulvarı 27310 Şehitkamil - Gaziantep, TÜRKİYE

ISSN

Table of Contents

A COMPARATIVE STUDY ON SEWAGE SLUDGE ASH AFFECTING MECHANICAL PROPERTIES OF GLASS FABRIC/EPOXY COMPOSITES

Mohamad Alsaadi[2], Ahmet Erkliğ[1]

[1]Gaziantep University, Faculty of Engineering, Mechanical Engineering Department, Gaziantep 27310, Turkey, erklig@gantep.edu.tr

[2] University of Technology, Materials Engineering Department, Baghdad 10066, Iraq, mohamad.alsaadi@mail2.gantep.edu.tr

ABSTRACT: The effects of sewage sludge ash (SSA) and silicon carbide (SiC) particles on the mechanical properties of S-glass fiber reinforced epoxy composites were investigated. Composite laminate samples for tensile and flexural were prepared and tested according to ASTM standards tests. The results showed that, the tensile and flexural strength were optimum at SSA content of 10 wt% by 8.4% and 33.1% compared to 1.5% and 24.2% with SiC content of 10 wt% and 5 wt%, respectively. Tensile and flexural modulus values of the composites were enhanced compared with the unfilled composite.

Key words: particle, polymer, fiber, mechanical properties.

INTRODUCTION

Polymeric materials have been used for a long time and continue to their important role today. Nevertheless, pure polymers have some limitations such as low strength and stiffness, hence their performance in various fields can be enhanced by adding rigid inorganic fillers in the common matrix resulting in increase of some mechanical properties like strength, modulus, toughness, etc.; furthermore, some of them can provide a significant cost reduction (Fu et al., 2008; Qinghua et al., 2015). Furthermore, particulate polymer composite are often limited from using in automobile, aviation, renewable energy construction and military application, accordingly glass fiber has the advantages of low cost compared to many fibers have been used in fabrication of composite laminates. therefore, using the glass fiber with particulate-filler modified polymer in order to produce cheapest composite laminates having wide applications and superior properties such as high stiffness, strength, thermal stability and resistance to chemical hurt (Sathishkumar et al., 2008; Patnaik et al., 2015). Thus, most polymer matrix has been usually used in these laminate composites is epoxy. Therefore, Epoxy matrix is modified by adding additional components, like thermoplastics (Van et al., 2014) and rubber fillers (Dadfar et al., 2013). For rubber particles, while the phase-separated structure in mixtures often raises the delamination resistance, the strength and modulus are reduced. Thermoplastics behavior the similar of

rubber filler do. Moreover, resin viscosity is greatly increased when high molecular weight thermoplastics are blended with epoxy resin, which causes processing difficulty. In addition, there are important factors strongly affected the mechanical properties of the particulate filled polymer composites, such as interfacial interactions and composite structure. Therefore, the production of good quality composite depends on the homogeneity and compatibility of filler within polymer matrix, which this can reduce the particle aggregation and improve the efficient of particle/matrix interfacial bonding energy and thus mechanical properties (Moczo J and Pukanszky, 2008).

Until most recently, researches focused mainly on rigid particles, like nano-silica, carbon nanotubes nano-clay, and nano-alumina (Wang et al., 2005; Coleman et al., 2006), due to their enhancement for mechanical properties of fiber/epoxy composite laminates. The strength of PEEK/AS-4 composite was significantly improved 12% by adding nano-silica particles of 1 wt% (Jen et al., 2005). Patnaik et al. (2009) found that the addition of FA and SiC micro-particles to glass fiber polyester composites significantly improved the flexural strength by about 10 wt% of FA content, while the tensile modulus increased for both fillers. Wang et al. (2016) raised flexural strength, impact strength values by 16% and 37%, respectively, by adding micro-particle of Al_2O_3 to the carbon fabric/epoxy composite. Bhagyashekar and Rao (2010) indicated that the addition of SiC particles having 44 μ particle size to epoxy was improved the tensile and flexural modulus of the epoxy/SiC composites. Some researchers have been used SSA as an industrial waste filler to improve some mechanical properties like tensile and flexural strength of the composites used for construction application such as bricks and tiles, as a raw materials for cement production, as aggregates for concrete and mortar (Smol et al., 2015). Hence, compared with the earlier studies, the addition of rigid inorganic particulate fillers may be modified for better prediction of the mechanical properties of the composite laminates. Therefore, it is more suitable to study the behavior of mechanical properties for the composite laminates containing micro- and nano-particles.

Population and plants growth increase wastewater in all over the world. Sewage sludge ash is generated during the combustion of dewatered SSA in a burner. SSA is stored and can be used as a filler material. One of the major environmental issues is eliminated some materials can give economical and sustainable solutions. SSA contains compound not harmful to the environments like oxides. The annual amount of SSA is about 3.5 billion m^3 in Turkey (TUIK, 2010). When the 4 percentage of this amount is considered as waste sedimentary, 140 million tons SSA potential is available in Turkey. Sewage sludge incineration system was first developed in Gaziantep (Kütük, 2013). System generates electric by burning approximately 150 tons SSA per day. About 15 tons ash remains at the end of combustion. When the established mechanism is thought as a recycling system the use of remain ash increase the value of mechanism and also use of ash can be regarded as a versatile earning due to its environmental problem. Applying of the SSA in the fabric/epoxy composites materials was examined in the present study.

Based on the above studies, many of these studies have investigated the flexural and tensile properties of the particulate fillers filled composite laminates. To the best of found knowledge, researchers in literature do not inspected the effect of SSA content on the mechanical properties of S-glass fiber reinforced epoxy (GFRE) composite. In this study, the mechanical properties (flexural and tensile) of GFRE composite were determined with the use of micro size SSA and SiC particles within epoxy matrix. In addition, the SSA and SiC variation of 5, 10, 15 and 20 wt% contents were incorporated with GFRE composites.

MATERIALS AND PROCEDURES

Materials

Epoxy (MOMENTIVE-MGS L285) and hardener (MOMENTIVE-MGS H285) were mixed with a weight ratio of (1/0.4) in the production of composite plates. Woven plain S-glass fiber with areal density of 200 g/m^2 were used as reinforcement fibers in the ply. All above materials were supplied by DOST Chemical Industrial Raw Materials Industry, Turkey. The fillers of SSA and SiC were supplied by Çatalağzı Power Plant, Şahinbey Belediyesi, Gaziantep, Turkey and Eti Mine Works General Management, Turkey, respectively. The particle size of the fillers was measured approximately 1-35 μm for grinded and garbled SSA filler and 35 μm for SiC filler. The bulk densities were measured: 0.72 and 1.49 gr/cm^3 for SSA and SiC, respectively, and their chemical compositions are given in Table 1.

Table 1. Chemical compositions of filler materials.

Filler	Chemical formula/Composition (wt %)
Sewage sludge ash	P_2O_5 (23.56), CaO (19.58), SiO_2 (16.6), SO_3 (8.53), MgO (8.22), Fe_2O_3 (7.46), Al_2O_3 (5.73), K_2O (4.87), ZnO (2.09), TiO_2 (1.08), Cl (0.54), Na_2O (0.44), Cr_2O_3 (0.24), BaO (0.21), CuO (0.19), MnO_2 (0.18).
Silicon carbide	SiC (100).

Composites production and samples preparation.

The composites were prepared by adding particulate SSA or SiC filler in epoxy resin with four different particle contents. The particulate filler quantity was mixed with epoxy with a constant speed of 750 RPM using a mechanical stirrer for 25 minutes to obtain a homogeneous particulate blend. Then hardener was mixed with particulate blend for quick setting of composite. Then, the particulate blend was applied to the fibers layer by layer until all the 16 layers were placed at room temperature 25°C. Afterward, modified laminated fabrics with dimensions of 160 mm×200 mm were subjected to 0.3 MPa pressure in the flat molds for 1 h curing time with 80 °C temperature. Afterward, laminate were cooled to the room temperature under the pressure (Lamination production process is shown in Figure 1). After the production composite laminates (In this work, the particulate composites will be referred to, for suitability as GFRE-SSA and GFRE-SiC), their sizes were cut to produce tensile and flexural specimens according to ASTM

standards. Figure 2 shows the tensile and flexural specimens of GFRE-SSA and GFRE-Si Composites with various particle contents.

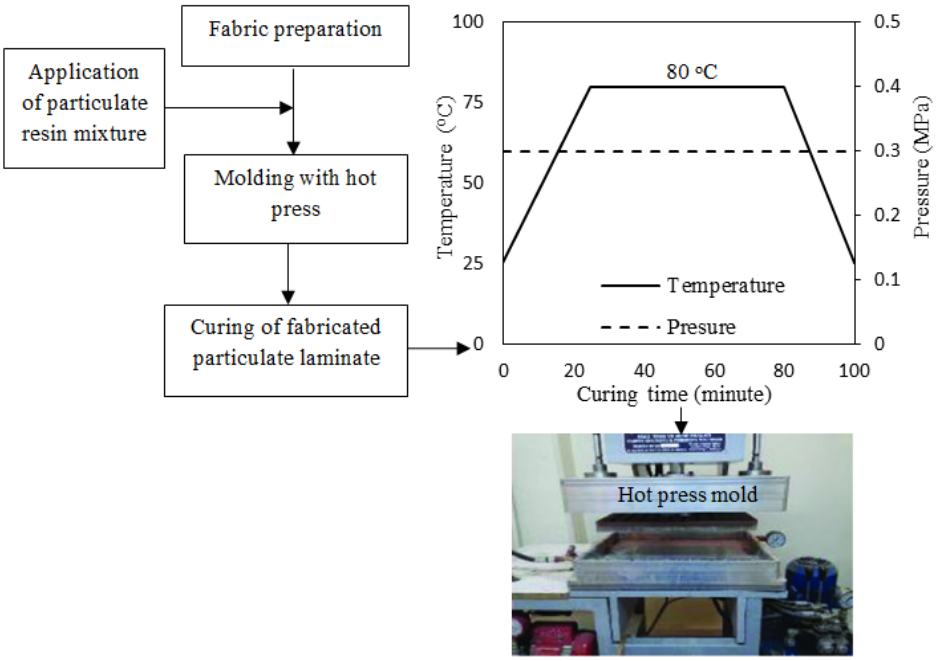

Figure 1. Production process and unit.

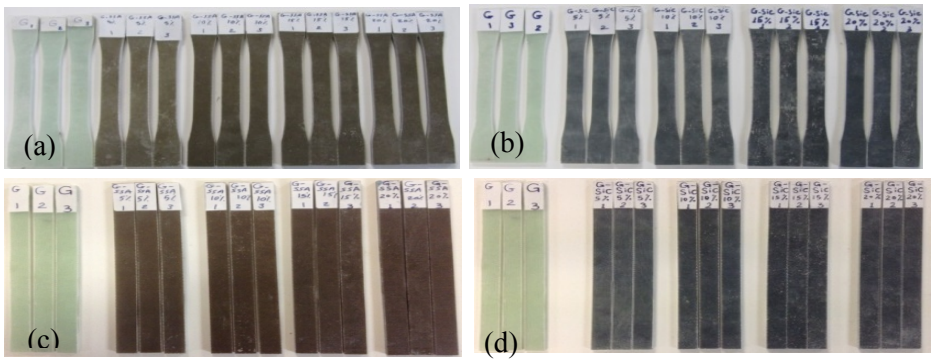

Figure 2. specimens of tensile test: (a) GFRE-SSA, (b) GFRE-SiC composites and flexural test: (c) GFRE-SSA, (d) GFRE-SiC composites.

Tensile and flexural tests

The tensile and flexural properties of the SSA and SiC particle-filled GFRE composite specimens were determined at room temperature using the Shimadzu testing machine AG-X series (Kyoto, Japan) and data acquisition card Ni-9237 (National Instruments Corporation, Austin, TX, USA) configuration (Figure 3). Tensile and flexural test samples were prepared according to the ASTM D 638(2010) in size of 165 × 13 mm for a gauge length of 50 mm and ASTM D 790 (2010) in size of 185 × 12.7 mm with span to thickness ratio of 32:1, respectively. All specimens had thickness in range of 3.4±0.3 mm due to particle content

variation. The crosshead speeds for tensile and flexural testing were 2 mm/min and 5 mm/min, respectively. At least three specimens were tested for each composite, and the average value of the output data was depended.

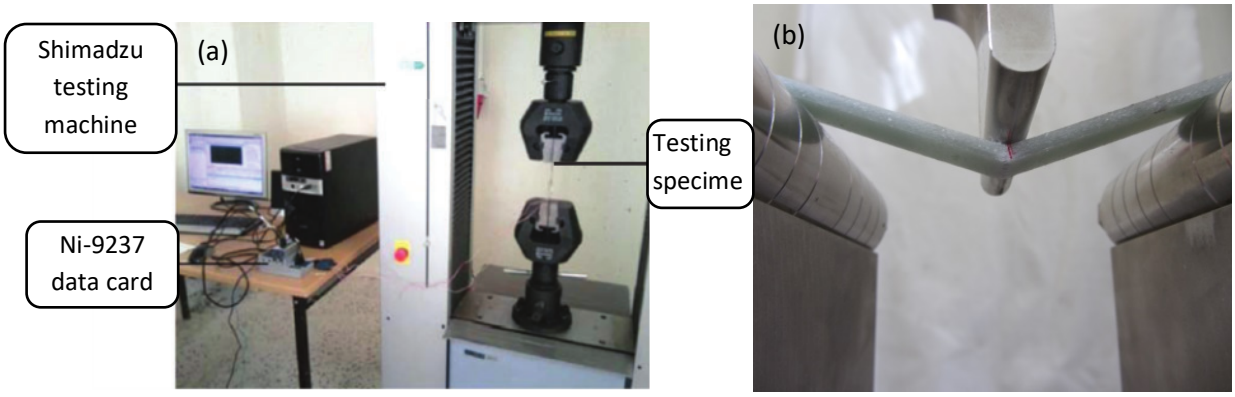

Figure 3. Shimadzu AG-X series testing machine (a) Tensile test, (b) Flexural test

RESULTS AND DISCUSSIONS

Effect of SSA and SiC contents on tensile properties

Table 2 displays the tensile properties of GFRE, GFRE-SSA and GFRE-SiC composites for various SSA and SiC filler contents. The tensile tests show a linear response of the elastic and the elastic plastic curves (Figures 4, 5) of the studied particulate composites, as shown in Figure 6, all the fracture surfaces of the samples were flat without any nicking, which means that the samples fail in a brittle manner when they were tested. Moreover, there was no effective permanent decreasing in samples' cross sectional area. Therefore, the samples of particulate composite exhibit a brittle behavior. In addition, whether it was filled or unfilled with SSA or SiC particles, the tensile samples were failed at higher stress. The tensile results show that, for the tested specimens of micro-particle filled GFRE composite, the tensile strength enhanced at 10 wt% content of, SSA and SiC, and then followed the trend of decreasing due to particle aggregation when the SSA and SiC addition above 10 wt%, forming stress concentration and thus weaknesses in the composite strength (Wang et al., 2016; Patnaik et al. 2009). The highest improvement of tensile strength was obtained at 10 wt% content of SSA and SiC with maximum increment of 1.5% and 8.4%, respectively.

Furthermore, the elongation at break decreased with the addition of SiC inorganic solid particles, while it increased with SSA addition due to the chemical compatibility of the SSA is better than SiC with composite system. Hence, the elongation at break improved by 18.2% with SSA addition compared to 4.3% with addition of SiC.

Moreover, as shown in Table 2, tensile modulus has been slightly enhanced by addition of SSA and SiC particles to the GFRE since rigid inorganic particles usually have much higher stiffness values than the organic polymer matrix. Hence, the composite modulus regularly increases with increasing particle content. The highest improvement of tensile modulus is obtained at 10, 5 wt% content of SSA and SiC with maximum increment of 5.2% and 9.4%, respectively, this difference may attributed to SiC particles have rigidity more than SSA particles . The Poison's ratio values of particulate GFRE change randomly with increasing particulate filler content, with slightly decreasing from unfilled GFRE composite.

Table 2. Tensile properties for the GFRE modified by SSA and SiC particles.

Composite type	Filler content (wt%)	Tensile strength (MPa)	Elongation at break (%)	Tensile modulus (GPa)	Poison's ratio
GFRE	0	389 (±15)	2.29 (±0.08)	19.1 (±0.62)	0.149
GFRE-SSA_5	5	391 (±11)	2.45 (±0.16)	19.3 (±0.15)	0.147
GFRE-SSA_{10}	10	422 (±16)	2.71 (±0.08)	20.1 (±0.37)	0.142
GFRE-SSA_{15}	15	386 (±14)	2.60 (±0.19)	19.8 (±0.60)	0.141
GFRE-SSA_{20}	20	370 (±8)	2.18 (±0.11)	19.0 (±0.29)	0.139
GFRE-SiC_5	5	374 (±12)	2.11 (±0.07)	20.9 (±0.19)	0.142
GFRE-SiC_{10}	10	395 (±17)	2.17 (±0.12)	20.5 (±0.48)	0.146
GFRE-SiC_{15}	15	354 (±9)	2.39 (±0.16)	20.2 (±0.20)	0.140
GFRE-SiC_{20}	20	344 (±11)	2.23 (±0.12)	19.8 (±0.15)	0.137

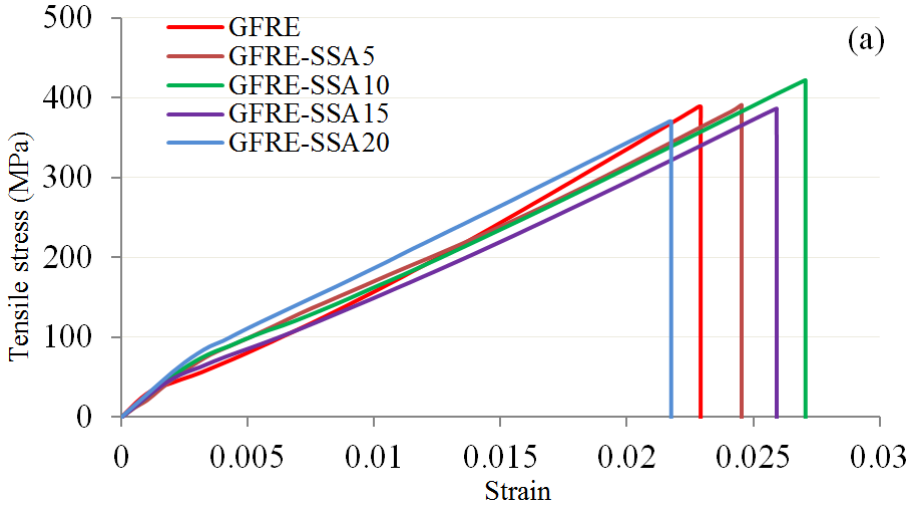

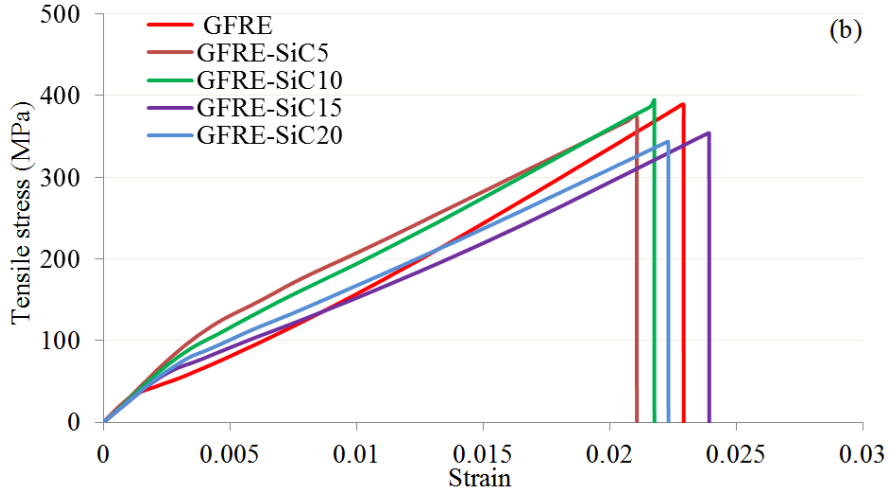

Figure 4. Tensile stress–strain responses for the composites: (a) GFRE-SSA and (b) GFRE-SiC.

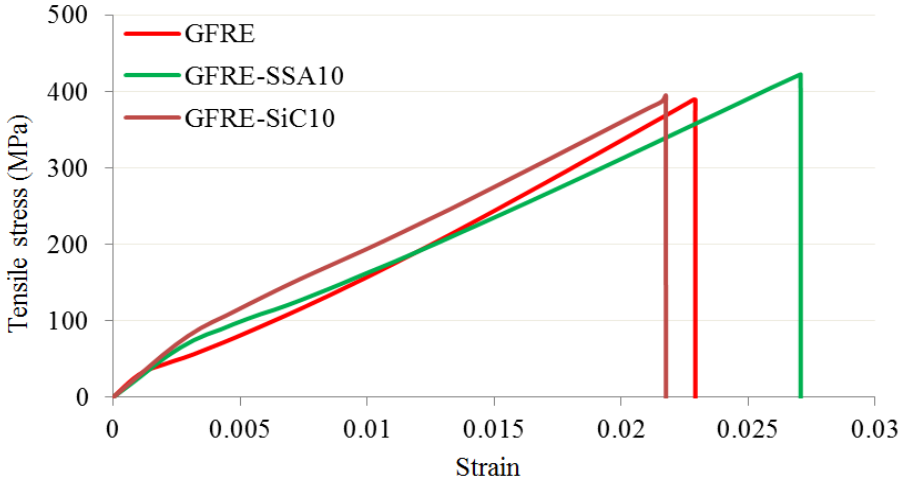

Figure 5. Comparison of tensile stress–strain responses according to composites have maximum strength.

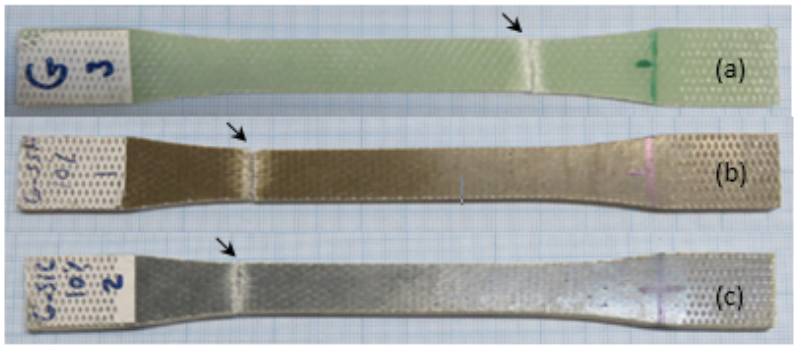

Figure 6. The failed specimens of maximum tensile strength for (a) GFRE, (b) GFRE-SSA and (c) GFRE-SiC composites.

Effect of SSA and SiC contents on flexural properties

The flexural test results are presented in Table 3, all the specimens of the micro-particle filled composite laminates have flexural strength higher than unfilled GFRE composites (Figure 7) Wang et al. (2016). In addition, the flexural strength increased from 410 MPa to 546 MPa when the content of micro-Bx particles changed from 0 wt% to 10 wt%, then further increasing the micro-SSA, the flexural strength reduced to 491 MPa. Same flexural strength trend was observed with addition of SiC particles. Therefore, the maximum increment was 33.1% at SSA content of 10 wt% compared to 24.2% at SiC content of 15 wt%.

The stress-strain responses of the GFRE, SSA-GFRE and SiC-GFRE composites obtained from three-point bending tests are shown in Figure 7. The stress-strain curves exhibited steadily increasing with a linear fashion. In addition, flexural specimens fail at higher stress, for unfilled and SSA or SiC particles-filled composites. In principle, the failure strain values of the GFRE specimens are increased by adding SSA and SiC micro size particles. Hence, the failure strain values increased by 22.5%, and 19.7% at particle content of 10 wt% SSA, 20 wt% SiC, respectively.

Moreover, the flexural modulus relatively improved with SSA micro-particle addition, which it was increased firstly from 2.08 GPa to 2.55 GPa and then decreased to 2.35 GPa, while the flexural modulus of the SiC-GFRE composites was less than unfilled GFRE composites. This behavior is clearly shown in Figure 8, in addition the linearity style of the stress-strain curve for SiC-GFRE composite is less than linearity of the unfilled GFRE and SSA-GFRE curves.

Table 3. Flexural properties for the GFRE modified by SSA and SiC particles.

Composite type	Particle content (wt%)	Flexural strength (MPa)	Failure strain (%)	Flexural modulus (MPa)
GFRE	0	410 (±19)	2.08 (±0.05)	21.0 (±0.32)
GFRE-SSA_5	5	501 (±22)	2.41 (±0.01)	21.6 (±0.85)
GFRE-SSA_{10}	10	546 (±25)	2.55 (±0.09)	21.7 (±0.36)
GFRE-SSA_{15}	15	520 (±9)	2.41 (±0.04)	22.2 (±0.62)
GFRE-SSA_{20}	20	459 (±14)	2.35 (±0.07)	20.9 (±0.14)
GFRE-SiC_5	5	422 (±15)	2.13 (±0.05)	19.3 (±0.40)
GFRE-SiC_{10}	10	440 (±7)	2.20 (±0.08)	18.7 (±0.09)
GFRE-SiC_{15}	15	509 (±16)	2.45 (±0.09)	19.6 (±0.20)
GFRE-SiC_{20}	20	476 (±24)	2.49 (±0.11)	18.1 (±0.75)

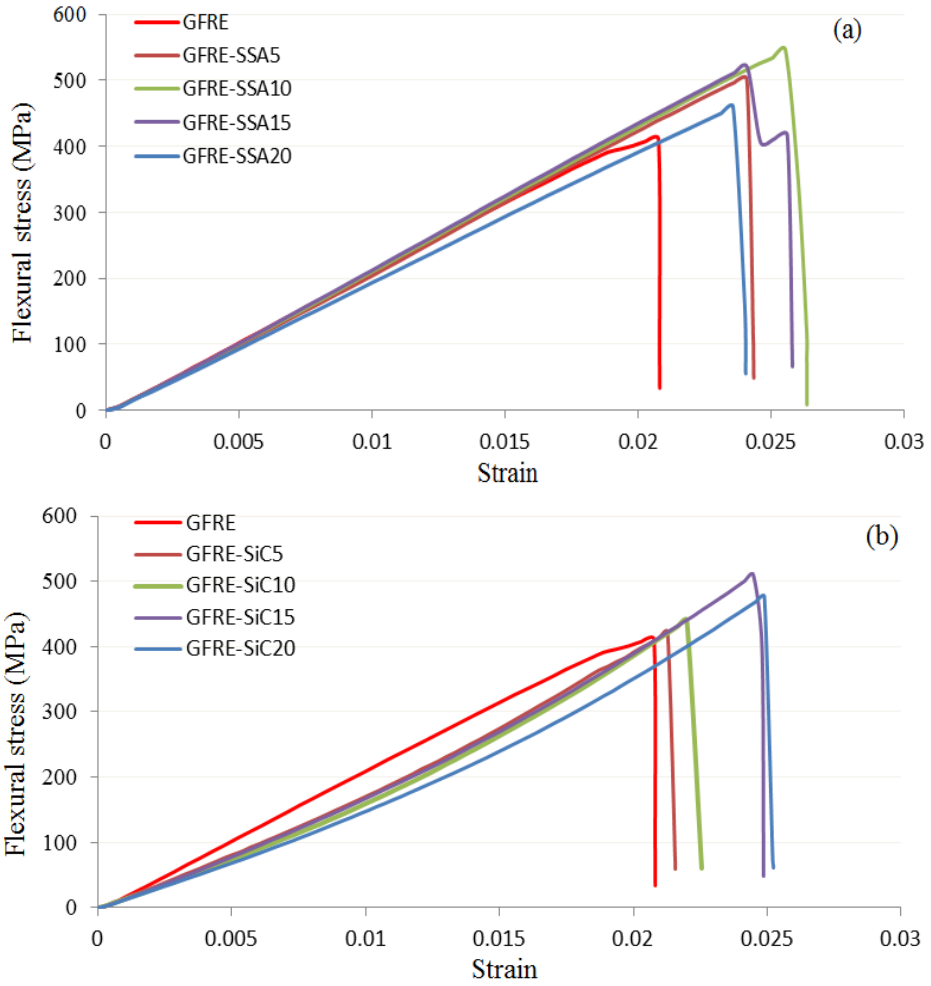

Figure 7. Flexural stress–strain responses for the composites: (a) GFRE-SSA and (b) GFRE-SiC.

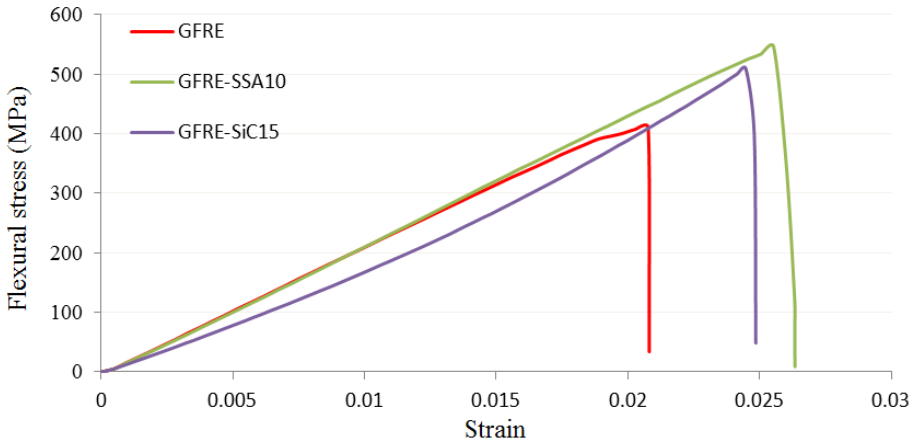

Figure 8. Comparison of flexural stress–strain responses for the composites have maximum strength.

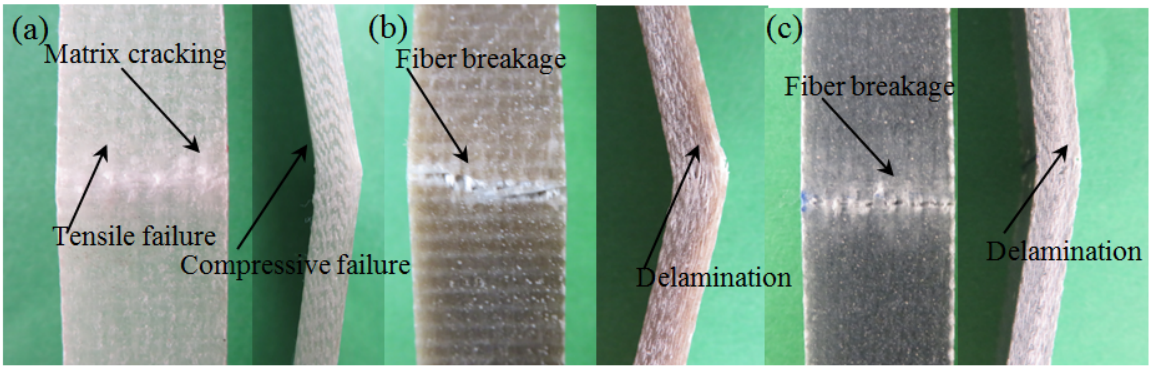

Figure 9. The failed specimens of the maximum flexural strength composites: (a) GFRE, (b) GFRE-SSA and (c) GFRE-SiC.

Flexural damage mechanisms of the GFRE, SSA-GFRE and SiC-GFRE composite specimens were characterized by taking pictures for the tension and side view of the fractured surfaces (Figure 9).The compressive and tensile failures are common failures under flexural loading and they include matrix cracking, fiber breakage and delamination (Davis et al. 2010). The failure of particulate-filled composite in flexural test is dependent on the maximum bending moment that the constituent materials can carry. Representative images for the tension and side view showed all these failure types. The tension views showed clearly the particulate-filled epoxy matrix cracking and the glass fiber breakage. On the other hand, side views illustrated the delamination of glass fiber plies.

CONCLUSIONS

The effects of sewage sludge ash industrial waste and silicon carbide ceramic particles with variation in contents on tensile and flexural properties of the glass fabric/epoxy composites were examined experimentally. The highest improvement of the tensile and flexural strength for GFRE-SSA composites was obtained at 10 wt% content, with a maximum increment of 8.4% and 33.1%, respectively. The tensile and flexural modulus was increased for all the GFRE-SSA composites and the highest improvement was at 10 wt% and 15 wt% content, with a maximum increment of 5.2% and 5.7%, respectively. Generally, the tensile and flexural failure strains of the GFRE-SSA composites were increased. All the above mechanical properties were better than unfilled GFRE and GFRE-SiC composites. Hence, this performance indicates the good adhesion strength and chemical compatibility of the SSA composite system. As a result, due to good mechanical properties and the lower cost of the GFRE-SSA composites, SSA industrial waste can be used as particulate-filler for polymer composites, and this the advantage of this study.

REFERENCES

ASTM D 638-10. (2010). Standard Test Method for Tensile Properties of Plastics; 2010.

ASTM D 790-10. Standard Test Methods for Flexural Properties of Unreinforced and Reinforced Plastics and Electrical Insulating Materials.

Bhagyashekar MS, Rao RM. (2010). Characterization of mechanical behavior of metallic and non-metallic particulate filled epoxy matrix composites. J Reinf Plast Compos; 29(1): 30-44.

Coleman JN, Khan U, Blau WJ, Gun'ko YK. (2006). Small but strong: a review of the mechanical properties of carbon nano tube polymer composites. Carbon; 44(9):1624–52.

Dadfar MR, Ghadami F. (2013). Effect of rubber modification on fracture toughness properties of glass reinforced hot cured epoxy composites. Mater Des;47(0):16–20.

Davis DC, Wilkerson JW, Zhu JA, Ayewah DOO. (2010). Improvements in mechanical properties of a Carbon fiber epoxy composite using nanotube science and technology. Compos Struct; 92(11), 2653–2562.

Fu SY, Feng XQ, Lauke B, Mai YW. Effects of particle size, particle/matrix interface adhesion and particle loading on mechanical properties of particulate–polymer composites. Composites Part B 2008; 39: 933–961.

Jen M-HR, Tseng Y-C, Wu C-H. (2005). Manufacturing and mechanical response of nanocomposite laminates. Compos Sci Technol; 65(5): 775–9.

Qinghua Q, Jianqiao Y. (2015). Toughening Mechanisms in Composite Materials. UK: Woodhead Publishin; 2015.

Moczo J and Pukanszky B. (2008). Polymer micro and nanocomposites: Structure, interactions, properties. J. of Industrial and Engineering Chemistry .

Kütük M. A. and Aksoy M. (2013). "A Case Study On Sewage Sludge Incıneratıon Plant: GASKI, " in Proceedings of the Second International Conference on Water, Energy and the Environment Kusadası, Turkey, 2013.

Patnaik A, Satapathy A, Mahapatra SS, (2009). Dash RR. A comparative study on different ceramic fillers affecting mechanical properties of glass-polyester composites. J Reinf Plast Compos; 28(11), 1305-1320.

Sathishkumar TP, Satheeshkumar S, Naveen J. (2009). Glass fiber-reinforced polymer composites – a review. J. Reinf. Plast. Comp. 33(13) 1258–75.

Smol M., Kulczycka J, Henclik A., Gorazda K., Wzorek Z. (2015). The possible use of sewage sludge ash (SSA) in the construction industry as a way towards a circular economy, J. Cleaner Production, 95, 45 – 54.

TUIK, (2010). "Municipals Waste Water Statistics," Turkish Statistical Institute.

Van der Heijden S, Daelemans L, De Schoenmaker B, De Baere L, Rachier H, Van Paepegem W, et al. (2014).Interlaminar toughening of resin transfer moulded glass fibre epoxy laminates by polycaprolactone electrospun nanofibres. Compos Sci Technol;104(19):6673.

Wang K, Cheng L, Wu JS, Toh ML, He CB, Yee AF. (2005). Epoxy Nanocomposites with highly exfoliated clay: mechanical properties and fracture mechanisms. Macromolecules;38:788–800.

Wang Z, Huang X, Bai L, Du R, Liu Y, Zhang Y, Zaho G. (2016). Effect of micro-Al contents on mechanical property of carbon fiber reinforced epoxy matrix composites. Compos Part BEng; 91:392–98.

WEAR PROPERTIES OF NANOFILLED AND MICROFILLED COMPOSITE RESTORARIVE MATERIALS

Efe Çetin YILMAZ[1*], Recep SADELER[2]

[1]Department of Technical Science of Pasinler Vocational School, Ataturk University Turkey, efecetinyilmaz@msn.com

[2]Department of Mechanical Engineering of Engineering Faculty Ataturk University Turkey, receps@atauni.edu.tr

*Corresponding Author

ABSTRACT: The purpose of this in vitro study was to compare the two-body wear resistance of nanofilled (3M ESPE Filtek Silorane) and microfilled (3M ESPE Filtek Z250) composite restorative materials. Eight standardized disc shape specimens (6mm diameter X 8mm height) were prepared from two composite materials. Specimens were subjected to chewing simulation using a chewing simulator (F=49N (vertical 6 mm, horizontal 2 mm) 2,4 X 10^5 cycles and frequency 1,6 Hz) and simultaneous thermal cycling (3000 cycles, 5°C/55°C, 1min/cycle). AL_2O_3 balls were used as antagonists for every experiment chewing cycle. Mean volume loss values were determined using 3D laser scanning device. Mean values and standard deviations were calculated and statistical analysis was performed using one-way Anova and Tukey's test (α=,05). Vicker hardness values for Filtek Z250 (about 69HV) and for Filtek Silorane (about 45HV) were measured. Mean volume loss of Filtek Z250 (3,8µm^3 p=.021) is measured to be lower than Filtek Silorane (5,9µm^3 p=.017). In this study, suggested the excellent two body wear behaviour of the microfilled Filtek Z250. However, this study isn't correlations linear between filler volume values and two body wear resistance

Key words: Two-body Wear, Composite Restorative Materials, Chewing Simulation, Thermal Cycling

INTRODUCTION

The use of light-activated resin composites has dramatically increased in the past years as a response to an increased demand for esthetic restorations.(Kurachi, Tuboy, Magalhaes, & Bagnato, 2001) Dental resin composites are heterogenous materials, usually consisting of three major components, namely resin matrix, inorganic fillers, and a silane coupling agent.(Bicer, Karakis, Dogan, & Mert, 2015) The amount and size of filler particles incorporated in the resin matrix determine the type, and ultimately, the most advantageous clinical application of each composite. Wear is the net result of a number of fundamental processes: abrasion, adhesion, adhesive effects between two contacting surfaces, fatigue and corrosive effects, which act in various combinations depending upon the properties of the

materials. Abrasion and attrition have largely been accepted as the primary clinical wear mechanisms for dental resin composites(Bicer et al., 2015; Harsha & Tewari, 2003; Heintze, Zellweger, Cavalleri, & Ferracane, 2006; Lim, Ferracane, Condon, & Adey, 2002). Wear of teeth and restorative materials is the result of different complex processes that depend primarily on the abrasive nature of food, the properties of the antagonistic material, the thickness and hardness of enamel, the chewing behaviour along with parafunctional habits, and neuromuscular forces.(Johansson, Haraldson, Omar, Kiliaridis, & Carlsson, 1993; Kim, Kim, Chang, & Heo, 2001; Mair, Stolarski, Vowles, & Lloyd, 1996) Therefore, it is clinically crucial issue to predict wear behavior of different composite restorative resins used in oral environment. Although most in vivo wear is three-body wear, however, wear at the occlusal contact areas (OCA) that stabilizes the vertical distance between the mandible and the maxilla is correlated with two-body wear simulations.(Bicer et al., 2015) Despite the improvement in wear resistance of restorative materials, wear continues to be a problem.(Bicer et al., 2015) Until recently, much of the published clinical data on composite restoratives have focused on generalized contact free abrasion (CFA) of the material.(Bicer et al., 2015) Although this type of wear pattern is clinically important, localized OCA wear, which is directly attributed to the presence of a contacting cusp on the occlusal restorations, may be of great concern.(Yap, Chew, Ong, & Teoh, 2002) A number of publications have suggested that OCA wear may be two to three times greater than CFA wear.(Lutz, Phillips, Roulet, & Setcos, 1984; Willems, Lambrechts, Braem, & Vanherle, 1993) If the amount of OCA wear, which may be accelerated by the chemical environment, is of sufficient magnitude appreciable changes in occlusion may develop.(Bicer et al., 2015) It has been demonstrated that dental restorative materials show different wear mechanisms under different in vitro wear conditions.(Hu, Shortall, & Marquis, 2002), and that none of the existing wear devices can simulate the clinical wear process completely realistically. (Condon & Ferracane, 1996) However, the clinical evaluation of wear is expensive and time consuming, and various important variables such as chewing forces or environmental factors cannot be controlled sufficiently.(Condon & Ferracane, 1996) Thus, despite of the complexity of the clinical wear processes, laboratory mastication simulation allows the investigation of single parameters of the wear processes, though it has to be borne in mind that even in vitro wear simulations show considerable variability.(Heintze, 2006) The objective of a laboratory simulation is to produce wear that correlates well with clinical performance and that can predict survival time.(DeLong et al., 2012; Souza et al., 2010) Ideal dental restorative materials yield wear resistance similar to that of tooth tissues. For improving the wear resistance of restorative materials and for minimizing filler exfoliation during wear processes, filler shape, size and volume have been modified extensively in the recent years (Christensen, 2007). In addition, several innovative dental restorative materials for application in posterior restorations have been introduced, featuring ormocer and Silorane technology. However, particularly for Silorane-based materials, the information on wear resistance that is available in the literature is very limited, and profound analysis of the wear behaviour of these materials has been demanded.(Christensen, 2007) Thus the purpose of this study is to evaluate effect

of two-body wear on microfilled(3M ESPE Filtek Z250), and nanofilled(Filtek Silorane 3M ESPE) composite restorative materials.

METHODS

Information provided by material manufacturers for materials used in this study are given in Table 1. A total of 16 specimens (6mm diameter and 8mm height) consisting of 8 specimens for each material were prepared following the manufacturer's instructions. All of the specimens were stored in distilled water for one week at 37 °C prior to two-body wear tests. In this study, a chewing simulation device designed to investigate dental materials was employed. The specimens and antagonists were mounted in chewing simulator using a ball-on-block design and were loaded pneumatically with vertical load of 49 N for 2,4 x 10^5cycles at a frequency of 1.6 Hz (1 mm lateral movement 2 mm mouth opening).

Table 1 Composite restorative materials used in this study

Materials	Manufacturer /Type	Filler	Matrix	Filler Volume(%)
Filtek Silorane	3M ESPE / Nanofilled	Quartz fillers, Yttrium fluoride	Siloranes	76
Filtek Z250	3M ESPE / Microfilled	ZrO_2, SiO_2	Bis-GMA, UDMA, Bis-EMA	60

RESULTS AND FINDINGS

One-way ANOVA indicated significant differences in Vicker hardness(HV) between the three restorative materials. Mean vicker hardness values ranged between approximately 49 and 69 HV were measured. (table 2)

Table 2 Vickers hardness of the restorative materials that were used in this study

Materials	Mean Vickers Hardness (SD)
Filtek Silorane	49,15(2,1)
Filtek Z250	69,25(1,4)

The results of the qualitative SEM analysis are presented in fig1 (respectively a: Filtek Silorane, b: Filtek Z250), showing image pairs of contact areas and wear track areas on specimens after chewing actions. Fig1(a) showed the contact area delineated by a sharp line from the polished specimen surface. However, Fig 1(b) which represents microfilled resin (Filtek Z250) showed significantly less wear of track by a sharp line from the polished surface than fig1(a) Filtek Silorane composite materials.

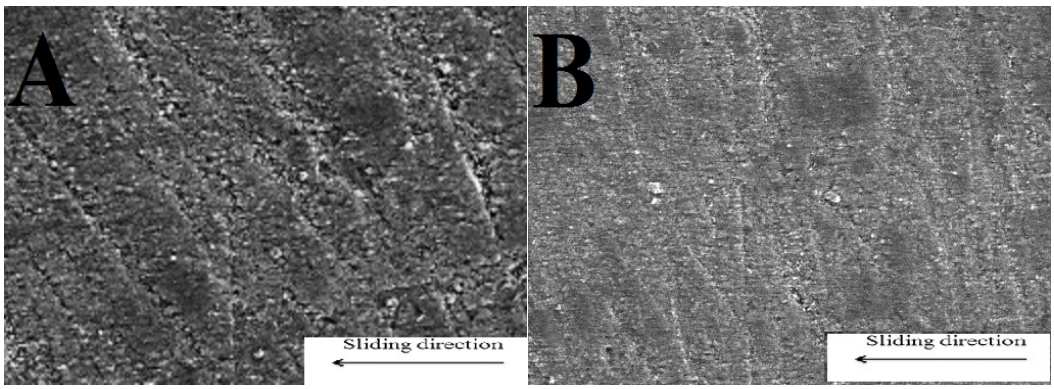

Figure 1. Respectively A:Filtek Silorane, B: Filtek Z250 (After 2,4X10^5 49 N chewing simulation and 3000 thermal cycles, 5°C /55 °C, 1 min/cycle)(HV:10kV mag: 500X 400µm)

Mean volume loss of Filtek Z250 (3,8µm^3 p=.021) is measured to be lower than Filtek Silorane (5,9µm^3 p=.017). In this study, suggested the excellent two body wear behaviour of the microfilled Filtek Z250. Moreover, each composite resin showed a distinct performance, which suggests that results were dependent upon each composite resin formulation. Other investigation has been reported that the filler particles play a particular important role for both hardness and wear resistance.(Cao, Zhao, Gong, & Zhao, 2013)The effect of filler volume on wear resistance follows a linear relationship, with high volumes decreasing wear rates due to lower expanse of resin unprotected by filler particles(Condon & Ferracane, 1997) which was supported by other researchers.(Heintze, Zellweger, & Zappini, 2007)However, regression analysis showed no correlation linear between filler volume values and two body wear resistance for the composite restorative materials investigated in this study. This can be explained as Filtek Z250 could most likely be attributed to the unique polymer structure which consist of well-dispersed microsize fillers.

It is difficult to reproduce the oral environment exactly in any two body wear testing system. Direct prediction of clinical wear resistance deduced from the present wear data results is thus not possible. Wear is a multifactorial process that probably cannot be described adequately with one material characteristic only (Koottathape, Takahashi, Iwasaki, Kanehira, & Finger, 2014). Thus further investigations is needed to examine characteristics such as three body wear, fatigue wear and fracture properties.

CONCLUSION

Within the limitations of this study, the following conclusions can be drawn: Among the composite materials used this study the microfill composite resin Filtek Z250 showed the least mean volume loss which was significantly lower than that of material of Filtek Silorane. Among the composite materials used this study

isn't correlations linear between filler volume values and two body wear resistance.

REFERENCES

Bicer, A. Z. Y., Karakis, D., Dogan, A., & Mert, F. (2015). A comparison of wear rate of direct and indirect resin composites: A two-body wear abrasion test. Journal of Composite Materials, 49(21), 2599-2607. doi:10.1177/0021998314550845.

Cao, L. Q., Zhao, X. Y., Gong, X., & Zhao, S. L. (2013). An in vitro investigation of wear resistance and hardness of composite resins. International Journal of Clinical and Experimental Medicine, 6(6), 423-430.

Christensen, G. J. (2007). Remaining challenges with Class II resin-based composite restorations. Journal of the American Dental Association, 138(11), 1487-1489.

Condon, J. R., & Ferracane, J. L. (1996). Evaluation of composite wear with a new multi-mode oral wear simulator. Dental Materials, 12(4), 218-226. doi:Doi 10.1016/S0109-5641(96)80026-1.

Condon, J. R., & Ferracane, J. L. (1997). In vitro wear of composite with varied cure, filler level, and filler treatment. Journal of Dental Research, 76(7), 1405-1411.

DeLong, R., Pintado, M. R., Douglas, W. H., Fok, A. S., Wilder, A. D., Swift, E. J., & Bayne, S. C. (2012). Wear of a dental composite in an artificial oral environment: A clinical correlation. Journal of Biomedical Materials Research Part B-Applied Biomaterials, 100b(8), 2297-2306. doi:10.1002/jbm.b.32801.

Harsha, A. P., & Tewari, U. S. (2003). Two-body and three-body abrasive wear behaviour of polyaryletherketone composites. Polymer Testing, 22(4), 403-418. doi:10.1016/S0142-9418(02)00121-6.

Heintze, S. D. (2006). How to qualify and validate wear simulation devices and methods. Dental Materials, 22(8), 712-734. doi:10.1016/j.dental.2006.02.002.

Heintze, S. D., Zellweger, G., Cavalleri, A., & Ferracane, J. (2006). Influence of the antagonist material on the wear of different composites using two different wear simulation methods. Dental Materials, 22(2), 166-175. doi:10.1016/j.dental.2005.04.012.

Heintze, S. D., Zellweger, G., & Zappini, G. (2007). The relationship between physical parameters and wear of dental composites. Wear, 263, 1138-1146. doi:10.1016/j.wear.2006.12.010.

Hu, X., Shortall, A. C., & Marquis, P. M. (2002). Wear of three dental composites under different testing conditions. Journal of Oral Rehabilitation, 29(8), 756-764. doi:DOI 10.1046/j.1365-2842.2002.00878.x.

Johansson, A., Haraldson, T., Omar, R., Kiliaridis, S., & Carlsson, G. E. (1993). An Investigation of Some Factors Associated with Occlusal Tooth Wear in a Selected High-Wear Sample. Scandinavian Journal of Dental Research, 101(6), 407-415.

Kim, S. K., Kim, K. N., Chang, I. T., & Heo, S. J. (2001). A study of the effects of chewing patterns on occlusal wear. Journal of Oral Rehabilitation, 28(11), 1048-1055. doi:DOI 10.1046/j.1365-2842.2001.00761.x.

Koottathape, N., Takahashi, H., Iwasaki, N., Kanehira, M., & Finger, W. J. (2014). Quantitative wear and wear damage analysis of composite resins in vitro. Journal of the Mechanical Behavior of Biomedical Materials, 29, 508-516. doi:10.1016/j.jmbbm.2013.10.003.

Kurachi, C., Tuboy, A. M., Magalhaes, D. V., & Bagnato, V. S. (2001). Hardness evaluation of a dental composite polymerized with experimental LED-based devices. Dental Materials, 17(4), 309-315. doi:Doi 10.1016/S0109-5641(00)00088-9.

Lim, B. S., Ferracane, J. L., Condon, J. R., & Adey, J. D. (2002). Effect of filler fraction and filler surface treatment on wear of microfilled composites. Dental Materials, 18(1), 1-11. doi:Doi 10.1016/S0109-5641(00)00103-2.

Lutz, F., Phillips, R. W., Roulet, J. F., & Setcos, J. C. (1984). In vivo and in vitro wear of potential posterior composites. Journal of Dental Research, 63(6), 914-920.

Mair, L. H., Stolarski, T. A., Vowles, R. W., & Lloyd, C. H. (1996). Wear: Mechanisms, manifestations and measurement. Report of a workshop. Journal of Dentistry, 24(1-2), 141-148. doi:Doi 10.1016/0300-5712(95)00043-7

Souza, R. O. A., Ozcan, M., Michida, S. M. A., de Melo, R. M., Pavanelli, C. A., Bottino, M. A., Martin, A. A. (2010). Conversion Degree of Indirect Resin Composites and Effect of Thermocycling on Their Physical Properties. Journal of Prosthodontics-Implant Esthetic and Reconstructive Dentistry, 19(3), 218-225. doi:10.1111/j.1532-849X.2009.00551.x.

Willems, G., Lambrechts, P., Braem, M., & Vanherle, G. (1993). Three-year follow-up of five posterior composites: in vivo wear. Journal of Dentistry, 21(2), 74-78.

Yap, A. U. J., Chew, C. L., Ong, L. F. K. L., & Teoh, S. H. (2002). Environmental damage and occlusal contact area wear of composite restoratives. Journal of Oral Rehabilitation, 29(1), 87-97. doi:DOI 10.1046/j.1365-2842.2002.00797.x.

ONE DIMENSIONAL MODELING OF GASOLINE ALCOHOL DUAL FUEL COMBUSTION ENGINE

Mustafa YILMAZ[1], Hasan KÖTEN[2], Ramin SAADAT POUR[3]

[1]Marmara University, Faculty of Engineering /Mechanical Engineering Department, mustafa.yilmaz@marmara.edu.tr

[2]Medeniyet University,Faculty of Engineering/Mechnaical Engineering Department, hasan.koten@medeniyet.edu.tr

[3]Marmara University, Faculty of Engineering /Mechanical Engineering Department, raminsaadatpour@yahoo.com

ABSTRACT: In this study, experimental outcomes from a Spark ignition engine (SI) which fueled with E1 to E20 (Percentage of alcohol content in total fuel blend is various between 1% and 20%) were collated with recital of combustion codes for one dimensional analysis.1-D codes, which is called SRM-Suite (Stochastic Reactor Model) and Chemkin-Pro, were estimated from combustion, emissions and heat transfer point in an SI engine. The estimations are based on empirical data and working situations which were done at karadeniz technical university Research Labs in Turkey. A bunch of empirical data was employed for analysis in both of software's according to both expanded and decreased kinetic mechanisms. Simulation outcomes were collated to empirical data from heat release rate, pressure and emission point. The vicissitude of the H_2O_2, temperature and OH which weren't available experimentally were achieved by comparisons between two codes. Analysis demonstrates that each code has pluses and minuses. The advantages of SRM-. Suite are blow-by Crevice, ring gap, and probability density function (PDF) – based stochastic reactor modeling and these advantages helped with better convergence of the outcomes. But, Chemkin-Pro outcomes were logical and solution duration was much shorter than SRM-.Suite. Also it was clear that both decreased and expanded kinetic mechanisms had huge effect on analysis.

Key-words: One-dimensional simulation, Chemical kinetic mechanism, SI engine, SRM-Suite, Chemkin-Pro.

INTRODUCTION

The expanded - mechanisms which has been set for fuels with high number of carbon commonly behold high number of elements and chemical reactions. By employing new generation of computers it's possible to achieve solution in very short period of time even for cases which have developed mechanisms [1]. During the past years' lots of computer engineers have tried to develop a software packages that be able to analyze 1-dimensional combustion to modeling of SI engines effectively. [2] One of the software's that was used in this study is

Chemkin-Pro which aim of its develop is to determine the accuracy of chemical mechanisms with evaluating of delay that happens in the ignition. Beside that its capable of doing analysis according to various reactor types. First one is a 1-D IC reactor. As the Chemkin-Pro software is capable of simulating engine combustion 1-D reactor, it is possible to be integrated with several zone models and CFD modeling to achieve much expanded numerical outcomes. Second one is SRM-Suite its 1-D codes for analyzing combustion the main aim for developing this software was to analyze SI engines according to probability density function (PDF) based on stochastic reactor model. The model works on assuming statistical uniformity of the blend inside the cylinder by factoring in the turbulent mixing [3][4].

Table 1. Nomenclature, Abbreviations
1-D → One Dimensional
3-D → Three Dimensional
CAD → Crank Angle Degree
CFD → Computational Fluid Dynamics
EGR → Exhaust Gas Recirculation
VC → Exhaust Valve Closing Time
EVO → Exhaust Valve Opening Time
HRR → Heat Release Rate
IC → Internal Combustion
IVC → Intake Valve Closing Time
IVO → Intake Valve Opening Time
ŁMM → Łocalness Mixing Model
PDF → Probability Density Function
PRF → Primary Reference Fuel
RPM → Revolution Per Minute
SRM → Stochastic Reactor Model
Symbols
a, b, c → Constants for Nusselt Equation
C_{11}, C_{12}, C_2 → Constants of Woschni Correlation
Nu → Nusselt Number
P → Instantaneous Cylinder Pressure (bar)
Pr, Vr, Tr→Volume, Temperature and Pressure Evaluated at any Reference Condition
Re → Reynolds Number
Sp → Piston Speed
Vd → Displaced Volume
$\hat{W}$ → Average Cylinder Gas Velocity

Here an SI engine was evaluated under two various mechanisms in the same working situation employing Chemkin–Pro and SRM-Suite software's results of both chemical mechanisms expanded for the same fuel were tested according their nearness to the empirical facts. Also, CPU analyzing times of codes were assumed as performance norm. To obtain the codes performances precisely, both decreased and expanded chemical kinetic mechanisms were employed [5]. In this study we

compared computational outcomes to empirical results from CO, O_2, CO_2, heat release rate and pressure point.

EXPERIMENTAL AND MODELING PARAMETER

Experimental part of study was carried out at Karadeniz Technical University Laboratories in the Turkey. The engine used in the tests is a single-cylinder, four-stroke, water-cooled, variable compression engine. Engine specifications are given in detail in Table 1. [6].

Table 2. Engine Parameters

Number	Characteristics	Values (Dimension)
Cylinder Diameter	90	mm
Stroke	120	mm
Łength Of Connecting Rod	140	mm
Compression Ratio	9.25	
Engine RPM	2000	Rev/min
Intake Valve Diameter	30	mm
Number Of Values	4	
Intake Valve Opening Time	340 BTDC	CAD
Intake Valve Closing Time	108 BTDC	CAD
Exhust Valve Opening Time	120 ATDC	CAD
Exhust Valve Closing time	322ATDC	CAD

To catch SI engine situation practically the head of piston was lifted to reach the compression ratio of 15.06 as well inlet temperate into the cylinder raised to 250 C^o. Experimental steps were done when the pressure of intake manifold was 1bar. RPM of engine was taken as2000 to obtain steady combustion. The ethanol content which used in alcohol–gasoline fuel in the engine was various between 1% and 20%. These studies done under two categories: first mechanism is decreased and second mechanism is expanded.

1D COMBUSTION MODELING

Combustion simulation was done using both SRM-Suite codes and Chemkin-Pro, under module of SI engine. All of the study were done between two times it starts at the closing time of intake valve and ends at the opening time of exhaust valve.

The compression ratio is 9.25 for Chemkin-Pro .
The proportion of length of connection rod to the radius of crank assumed is 1.58.
Operating criterions were chosen on 2000 RPM .
Equivalent values were employed for decreased and expanded mechanisms and the test steps assumed as 0.1.
The temperature of inlet blend was assumed as 450 for reduced mechanism and for detailed mechanism it was assumed as 530k.

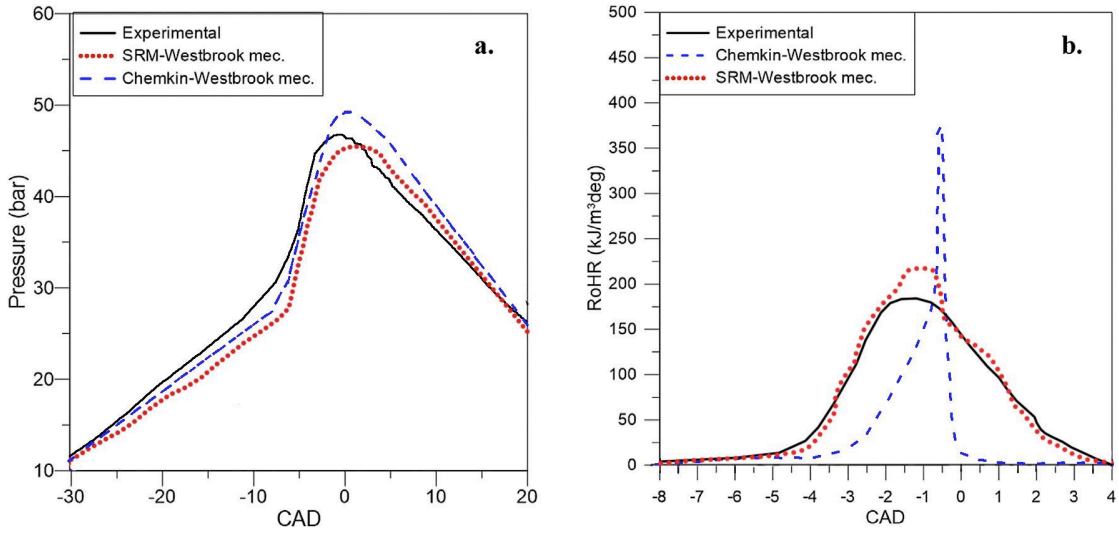

Figure 1. (i) Pressure Diagram Of Empirical And Simulating With Expanded Mechanism. (ii) Empirical And Simulating With Expanded Mechanism Of Heat Release Grade Diagrams

The pressure of intake assumed as 1.43 bar according to empirical information. The following equation was employed for simulating the heat transfer: [7]

$$Nu=a \times Re^{b} \times Pr^{c} \qquad (1)$$

According former researches for an SI engine constant parts of equation are assumed as:

a=0. 32, b=0.69, c=0.001.

The temperature of cylinder boundary parts was assumed as 420 K.

The Chemkin-Pro employs woschini relations to calculate heat transfer:

$$W=c_1 \times s_p + c_2 (V_d \times Tr/P_r \times V_r)(P-P_m) \qquad (2)$$

For a SI engine constants are assumed as C_{11}=2.28 , C_{12}=0.308 ,C_2=3.24.

SRM -Suite models were arranged and modeled also within the time interim of the closing of intake valve and opening of exhaust valve .

The data entered in Chemkin-Pro assumed same with data entered in SRM-Suite modeling.

110 particles were employed to decently evaluate inside-cylinder feature and also weight factor assumed as 13. The time for mean mixing assumed as 5.5 ms also localness mixing model (ŁMM). is specifically suggested for SI engine demands because it factors in localness into calculation [8].

RESULTS

In expanded mechanism case entire time that CPU needed was 123,016 s and in decreased case it was 2851s for SRM-Suite software. It's totally different when we used Chemkin-Pro software for expanded case it was 3050 s and for decreased case it was 355 s. estimated out comes were tested compared to heat release rate pressure–crank angle change, temperature and mole fractions of C_2H_5OH, C_8H_{18}, CO, CO_2, H_2O and OH [9]. Empirical outcomes were collated to estimated data from heat release rate, pressure, temperature and fractions of CO, CO_2, and O_2 point. The data that isn't accessible empirically like C_2H_5OH, C_8H_{18}, CO, CO were obtained by employing computational amounts also variation of H_2O_2 and OH, that are middle species in SI combustion, were shown graphically by employing computations. In figure 1. i it's obvious that expanded case from peak pressure point, SRM-Suite has much better consistency with empirical data in pressure vs crank angle diagrams compared with Chemkin-Pro. Figure1. ii demonstrates the empirical heat release value against crank angle and estimated outcomes of expanded mechanism by employing SRM-Suite and Chemkin –Pro It's obvious in figure SRM-Suite outcomes are in much better compliance from inclinations and rates point than Chemkin-Pro when collated to empirical outcomes.
It's clear in figure 2 i that the decreased mechanism outcomes demonstrate less proper results than expanded mechanism when collated to the empirical outcomes, SRM - Suite and Chemkin - Pro pressure vs crank angle diagram demonstrates this fact that combustion began afterwards, but occurred faster when collated to the empirical results. If we analyze Figure 2. ii it demonstrates stalled and quicker burning in computational estimations. Broadly, from heat release rate and pressure point computational outcomes achieved by the expanded mechanism demonstrated better compliance with empirical out comes [10]. From heat release rate point SRM - Suite out comes demonstrated more consistency than Chemkin–Pro. In addition, both Chemkin - Pro and SRM - Suite run on the same basic correlations the major disagreement among them is the significant participation of stochastic on results. Chemkin-Pro presumes that gas temperature stays uniform at the whole burning chamber so assumption results in abrupt pressure increase [11]. Beside this burning processes happen quicker compare with empirical actions due to the erasure of lots of middle reactions to decrease the CPU time remarkably. This process results to abrupt pressure increase and the variation in heat release grade [12]. Even so because of the effect of the decreased mechanism on CPU time it's possible to ignore the deviation. Figure.3 demonstrates computational increasing of

temperature during the burning process. At most temperature for combustion values are among 2000K and 2100K. Figure.4 demonstrates depletion of fuel for each of pieces C_2H_5OH and C_8H_{18}. In case of decreased mechanism (Tsurshima), fuel was used rapidly and finished steadily. The reason for rapid fuel depletion of the decreased mechanism is lack of middle reactions. [13] It worth to say that whole of calculational studies demonstrated the same duration of time for depletion of fuels. Figure.5 demonstrates variation of CO andCO_2 vs crank angle. Commonly, the outcomes demonstrated identical tendency apart from the cases running on SRM-Suite expanded mechanism. It's not possible to test the exactness of the outcomes by collating with other results destitute of reasonable empirical values[14]. Figure 6. demonstrates variation of OH and H_2O vs crank angle. While curves are analyzed it's clear that mole fraction of OH varied for two mechanisms SRM-Suite expanded mechanism studies demonstrated faster appraisal of OH which has less apogee amount [15].

Mass portion of H_2O_2 vs crank-angle obtained before, throughout and later than burning in an SI engine by employing empirical results. Empirical results were in concession with SRM-Suite Studies employing the method of Tsurushima. [16] Also the calculation outcomes for H_2O_2 were impossible to be ratified empirically. It is clear the alternation of SRM-Suite expanded mechanism demonstrated in CO, CO_2 and OH point is impossible to be seen in H_2O_2 [17]. It's obvious in Figure.6 ii, the developing of H_2O_2 starts in advanced compared with modeling with decreased method. As the consuming duration of H_2O_2 is approximately equal for whole studies, it indicates the ignition stall of engine overlap [18]

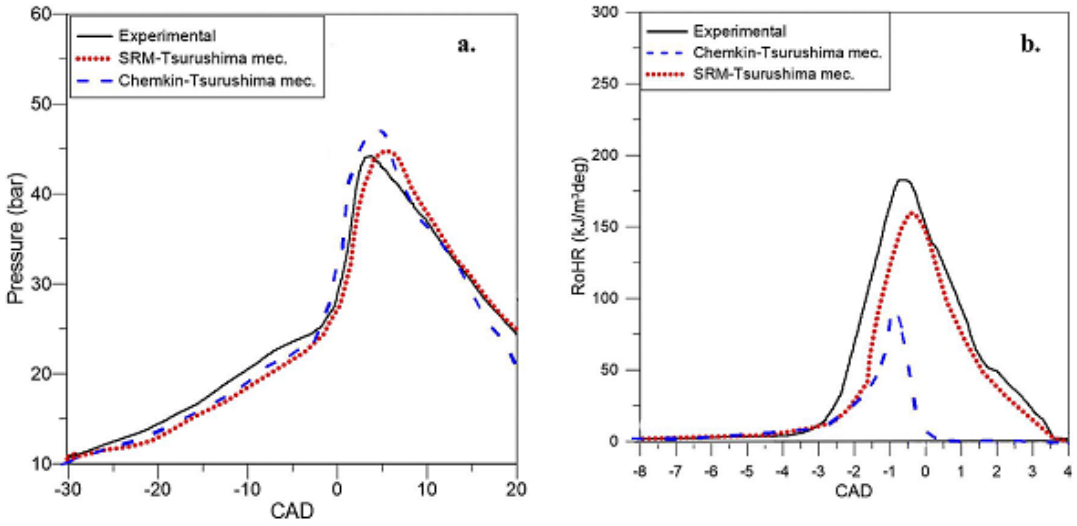

Figure. 2. (i) Pressure Diagram From Empirical And Simulating By Decreased Mechanism. (ii) Empirical And Simulating By Decreased Method Of Heat Release Grade Diagrams

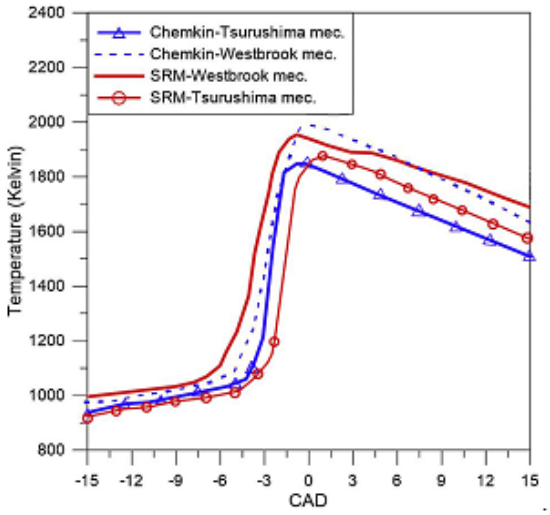

Figure. 3. Temperature Diagrams

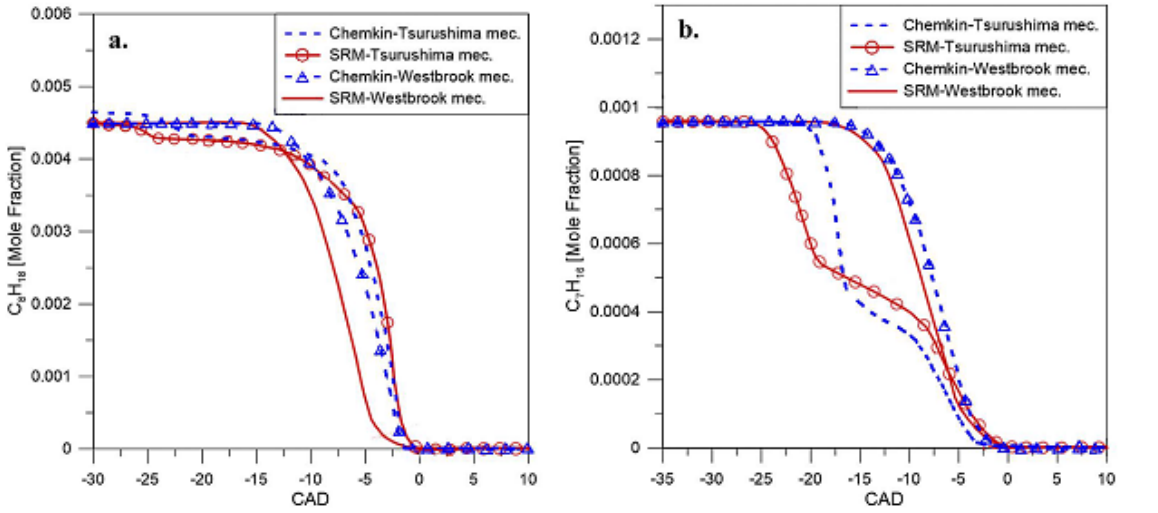

Figure. 4. C_2H_5OH (i) And C_8H_{18} (ii) Fuel Depletion Diagrams For Various Dissolvers Also Chemical Method Relaying On CAD.

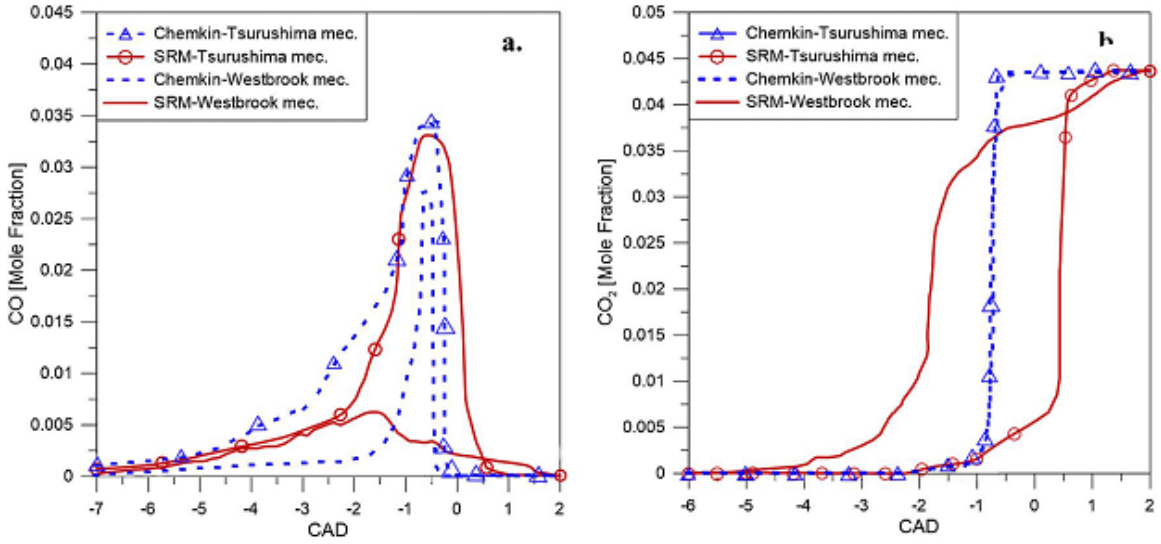

Figure. 5. CO (i) And CO_2 (ii) Diagrams For Various Dissolvers As Well Chemical Methods Relaying On CAD

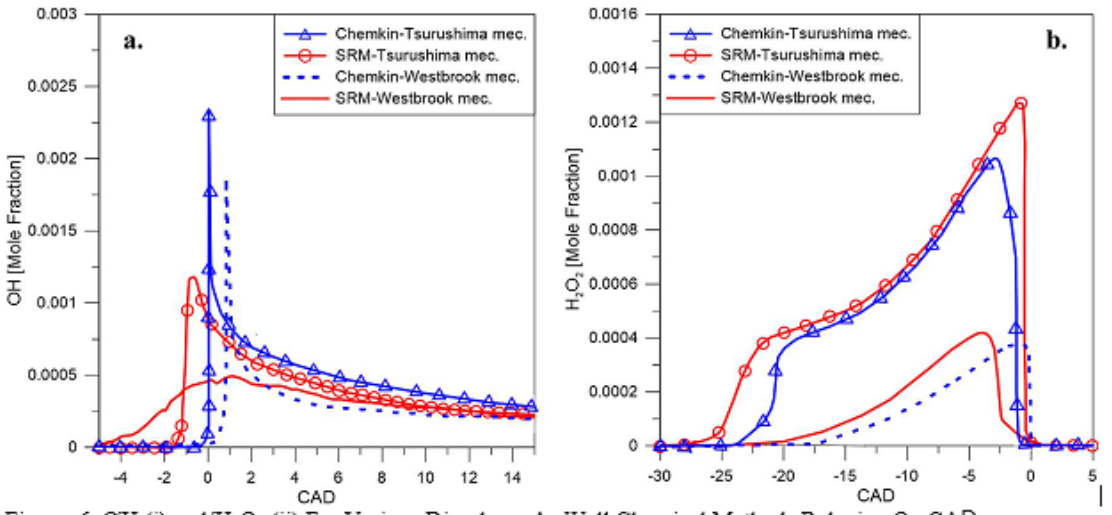

Figure. 6. OH (i) and H_2O_2 (ii) For Various Dissolvers As Well Chemical Methods Relaying On CAD

In Figure.7 empirical and some estimational outcomes of CO, CO_2 and O_2 are demonstrated. In CO case, Chemkin-Pro demonstrated better concession with the empirical data compared with SRM-Suite for either decreased and expanded methods. In CO_2 and O_2 case, whole estimated outcomes are in agreeable compliance with empirical outcomes.

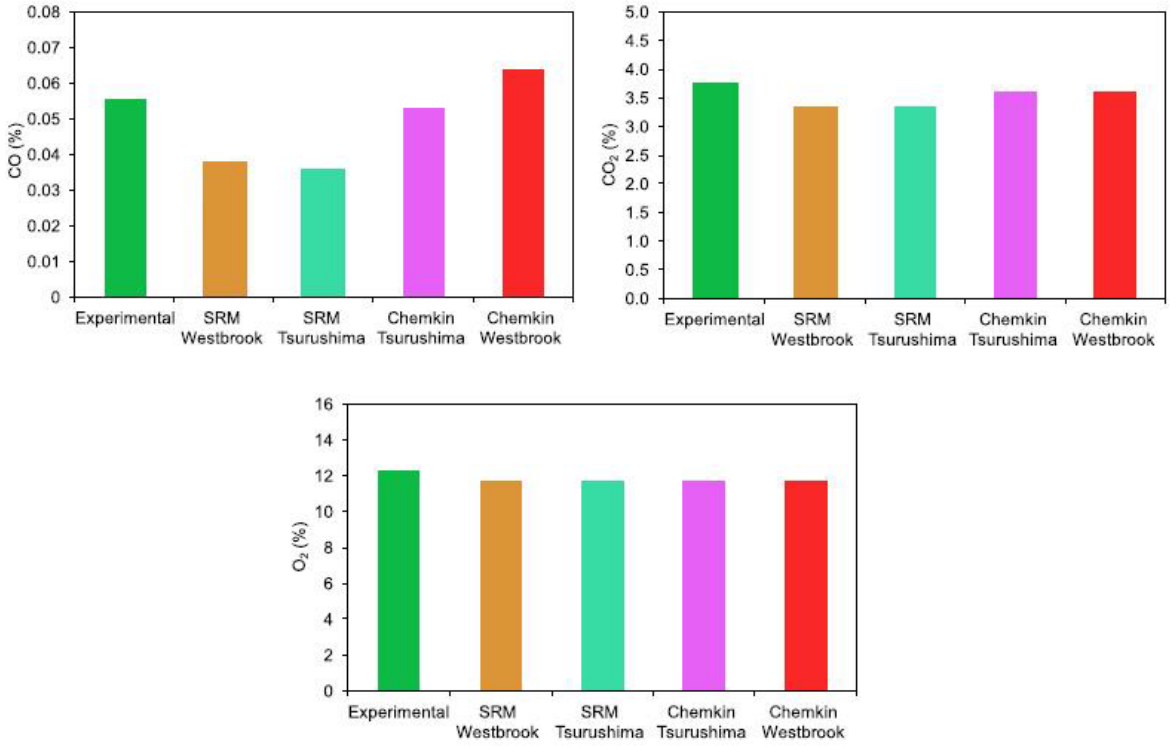

Figure. 7. Empirical And Estimated Amounts Of CO, CO_2, And O_2.

CONCLUSION

In this study I have researched and optimized the effect of fuel ethanol in gasoline combustion engines from emission and performance point. At the first level, I surveyed the engine performance for pure gasoline fuel; then I used a mixture of ethanol and gasoline in which the amount of ethanol varies from 1% to 20 %. The engine RPM was chosen as 2000 and the engine parameters, when it works with 100% gasoline fuel, were compared to when ethanol-gasoline fuel were blended. From the performance and emission value points it was obvious that 8% ethanol-gasoline blend is the desirable amount. It is clear that from performance and CO point, there is a good agreement between the results and literature researches. From performance and emission point it can be easily perceived that the gasoline-ethanol blend has advantages over pure gasoline. However, for obtaining the most decent value of gasoline-ethanol blend all of the engine parameters should be evaluated in an advanced optimization software in which the meantime factors in the gasoline-ethanol such as cost, engine performance and emission. If this conditions are met this study will be useful and practical.

In this study all of the engine parameters were defined variable, at the same time, engine performance and emission values were optimized together.
If renewable sources are used to produce ethanol the cost of product will be high. Despite this, it is preferable to use gasoline-ethanol blend from performance and

emission point under aforementioned conditions since passenger cars emissions have turned to be the main problem in air pollution and governments, therefore, pass strict rules about passenger cars which result in emission every year. From software point of view each, SRM-Suite and Chemkin-Pro have pluses and minuses: The major strong point of SRM-Suite codes is that it employs PDF method that ease CFD procedure when it sustains estimation ability of three dimensional CFD codes. Chemkin-Pro software presumes a bulk volume empirical outcomes. SRM-Suite factors in simulation of piston position and blow-by, so it makes possible to give better estimation outcomes when collated to Chemkin-Pro.

Also if we go through results it's obvious that expanded mechanisms are more sustainable and near to empirical data from intake temperature and emissions point nevertheless the expanded method has some weak points. One is that it rises CPU time it's different for both codes .in fact the expanded method rises CPU time up to 10 times for Chemkin-Pro and almost 100 times for SRM-Suite.

REFERENCES

Ahmed, S. (2013). Effect of Methanol – Gasoline Blends on S.I. Engines Performance and Pollution. Mechanical & Mechatronics Engineering, 13,5-15

Anderson,J.E.,DiCicco,D.M.,Ginder,J.M.,Kramer,u., Leone, T.G., Raney-Pablo, H.E & Wallin&gton, T.J. (2012). Quantifying the potential benefits in the United States. Fuel,97, 585-594

Battin-Leclerc, F. (2008). Detailed chemical kinetic models for the low-temperature combustion of hydrocarbons with application to gasoline and diesel fuel surrogates. Middle east journal of scientific Research, 4,429-431.

Feng, R.Yang,J.,Zahng,D.,Deng,B.,Jiangin,F.Liu,J. & Liu,X (2013). Experimental study on SI engine fuelled with butanol–gasoline blend and H2O addition .,. Journal of Energy conversion and management, 74,192-200.addition ,Energy conversion and management, 74,192-200.

Fröjd, k. P. (2012). 1D engine modeling with detailed reaction kinetics. Journal of Swedish and Finnish National Committees of the International Flame Research Foundation,17, 233-228.

Bayraktar, H. (2005). Experimental and theoretical investigation of using gasoline–ethanol blends in spark-ignition engines. Renewable energy, 30, 1733-1747.

He, B., &Zhao,H. (2015). Comparison of combustion characteristics of n-butanol/ethanol–gasoline blends in a HCCI engine. Energy Conversion and Management, l95 pp 101-109.

Iliev, S. (2015). A Comparison of Ethanol and Methanol Blending with Gasoline Using a 1-D engine Model. Procedia Engineering., 100, 1013-1022.

Kumar, K. .. (2014). Autoignition response of n-butanol and its blends with primary reference fuel constituents of gasoline, Combustion and Flame,162, 2466-2479.

Masum, B., Masjuki,H.,Kalam,M.,Fattah,M.,Palash,S. &Abedin,M. (2013). Effect of ethanol–gasoline blend on NOx emission in SI engine . Renewable and Sustainable Energy Reviews, 24, 209-222.

Manzetti, S. (2013). Background for new guidelines for emission control. Fuel, 140 ,293-301.

Najafi, G., Tavakoli,T.,Yusaf,F., & Faizollahnejad M (2008). Performance and exhaust emissions of a gasoline engine with ethanol blended gasoline fuels using artificial neural network. Applied Energy, 86 630-639.

Najafi, G., Ghobadian ,B., Yusaf, T., Ardebili ,S. & Mamat, R.. (2014). Optimization of performance and exhaust emission parameters of a SI (spark ignition) engine with gasoline-ethanol blended fuels using response surface methodology. energy, 110 ,1-15.

Neroorkar, K. a. (2011). Modeling of vapor-liquid equilibrium of gasoline-ethanol blended fuels for flash boiling simulations. Journal of Fuel,90,665-673.

Pathre, A. F, & Pathre,P.A. (2012). Experimental Investigation of Methanol, Ethanol and Butanol Blends with Gasoline on Si Engine. International Journal of Emerging Technology and Advanced Engineering, 2 ,2250-2459.

Wang ,Y.,Yao,M. &Zheng,M. (2013). A semi-detailed chemical kinetic model of gasoline surrogate fuel for internal combustion engine applications. fuel,113,347-356.

Zahang, C. & Shen, P. K. (2011). The simulation based on CHEMKIN for homogeneous charge compression ignition combustion with on-board fuel reformation in the chamber. international journal of hydrogen energy 37, 446-4475.

Zhang, Z.,TY,W., & XZ,M.(2014). Combustion and particle number emissions of a direct injection spark ignition engine operating on ethanol/gasoline and nbutanol/gasoline blends with exhaust gas recirculation. fuel,130,177-188.

IMPLEMENTATION OF WIRELESS ENERGY TRANSMISSION ON MOBILE ROBOTS

Mehmet Ali Özçelik
Gaziantep University, Technical Science, Electric and Energy Dep., Gaziantep, Turkey

ABSTRACT

The wireless energy transmission is becoming widespread every day. In this study, this technology is applied to a mobile robot. The energy received from the grid is transferred to the mobile robot and the entire system on the mobile robot works with this transferred power. Thanks to the mobile ability of the mobile robot on the line, unmanned transportation, stocking, production can be done. The system is designed to be used safely during the day without the need for maintenance and repairs because it operates without an integral power unit and contributes to the factory production system.

Keywords: Wireless energy transmission, resonance, magnetic flux

1. INTRODUCTION

Wireless energy transfer has been in the forefront recently, due to its wide application potential in the electronics industry [1-2]. Power supply can be provided by wireless energy transfer applications such as medical circuit applications, charging sensor connected to high voltage transmission lines where energy supply by cable is dangerous or not possible [3] as well as wireless energy transfer in the development of electric vehicle and battery technology [4].

By the time a conduction electric current is applied, a circular electromagnetic field is formed around the conductor. When the conduction is made into a conductive ring, the electromagnetic field that is formed becomes larger. Increasing the number of rings will lead to an increase in the magnetic field. When another ring conductor enters the effect area of the magnetic field, a voltage is induced on this conductor and an electric current is generated. This state is defined as inductive coupling. A typical conversion chain in a charging system formed by the principle of inductive coupling is shown in Fig.1.

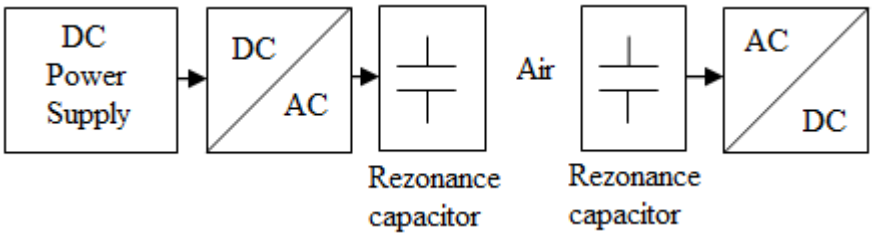

Figure 1. Conventional wireless energy transfer

The resonant capacitor circuits formed of the transmitting part and the receiving part mutually transmit the energy to the receiving side by the transmitter at a certain frequency value and electromagnetic field interaction while being in the mutual interaction area. Fig. 2 shows the equivalent circuit of a transformer, the battery in Fig. 1 match the AC / DC rectifier RL load resistance in Fig.2.

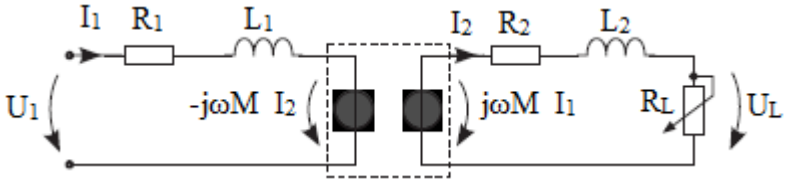

Figure 2. Transformer equivalent circuit

The coils of the receiver and transmitter are the same type and the common coil of the transmitter coil is switched to give two separate magnetic fields in opposite directions, the direct current (DC) at the transmitter input is passed to the alternating current (AC) the field is coming to fruition. When this variable magnetic field is thought of as the air transformer cores between the receiver and the transmitter, it cuts off the secondary winding of the receiver circuit and the magnetic field brings the AC voltage on the seconder winding or the receiver unit. It is converted to DC norm with AC / DC rectifier in receiver circuit. Fig. 3 shows the transmitter output, receiver input voltage signals in the wireless energy transmission application device.

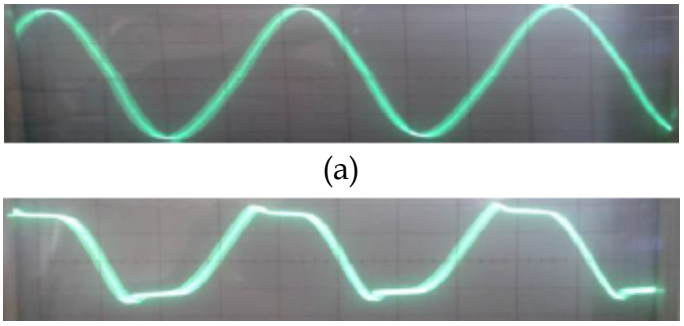

(a)

(b)

Figure 3. Transmitter circuit (a) voltage output, receiver circuit (b) voltage input signals

The distance between the transmitter and the receiver affects the efficiency of the wireless energy transmission considerably, and the yield is given in equation (1). Where η is the input voltage, Vi is the input voltage, V_s is the supply voltage, V_0 is the output voltage, Pi is the input power, P_0 is the output power of the system, R_s is the system resistance, R_0 is the load resistance.

$$\eta = \frac{P_0}{P_i} x100\% = \left(\frac{V_0^2}{R_0}\right) / \left(\frac{V_s - V_i}{R_s}\right) x V_i \quad (1)$$

2. EXPERIMENTAL SETUP

The block structure of the experimental system is shown in Fig. 4, while two test robots were run on a 60x60 cm plywood power surface, which provides wireless two-way communication, followed by a line and consuming 200mW each. In the system there is no battery in the robots moving on the line, infrared sensor is used as the sensor in the line monitoring circuit.

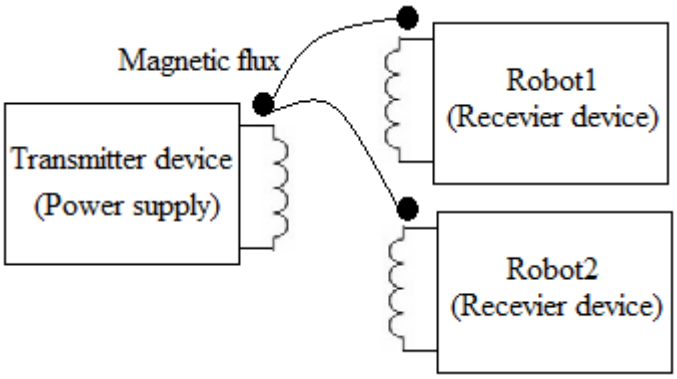

Figure 4. Power supply and receiver block diagram

On the back surface of the 60x60cm plywood, there is a transmitter circuit and a resonance coil, the resonance coil number turn of the transmitter circuit is 23 and the inductance value is 740H, the oscillation frequency of the transmitting circuit is 112 kHz and the resistance measured at the direct current is 0.42 Ω, the crystal quality coefficient Q = 2πFL / R = 1240. The transmitter circuit is shown in Fig.5 Here, two mosfets and drive integrations are used and AC is obtained from the common winding resonance coil.

Figure 5. Transmitter Device

A top view of the receiver circuit is shown in Fig. 6, a bottom view is shown in Fig. 7, wherein the receiver coil and the transmitter coil have the same electrical characteristic, the voltage is generated on the receiving coil because it is cut off by the magnetic flux composed in the transmitting coil. A suitable efficient receiver is obtained by designing the appropriate coil and capacitor resonance circuit for the frequency received on the receiver side. The receiver device is also a line-following robot circuit, and the main circuit is equipped with a PIC 16F628 microcontroller, motor drive circuit, sensor outputs. The output voltage of the receiver device is implemented on two BDX53 darlington transistors. By this way, two unit 6 V 150 rpm DC motor and microcontroller circuit have been operated. The device is built on epoxy printed circuit board.

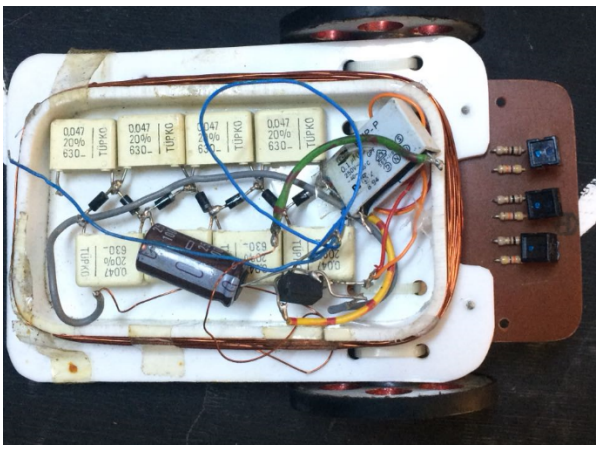

Figure 6. Receiver (robot) circuit top view

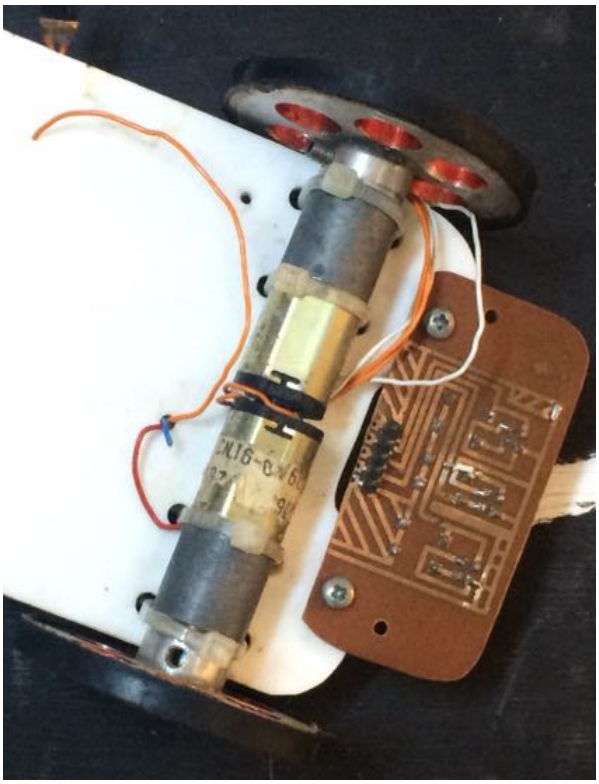

Figure 7. Receiver circuit bottom view

In Figure 8, the sensor track is seen, the transmission of white color is provided by means of 4 infrared ray sensors and the robot moves on this route. The microcontroller location information is provided by sensors here. The data from the sensors is checked by the algorithm in the microcontroller to control the motor drives at the output. The flow diagram of the algorithm is given in Fig.9.

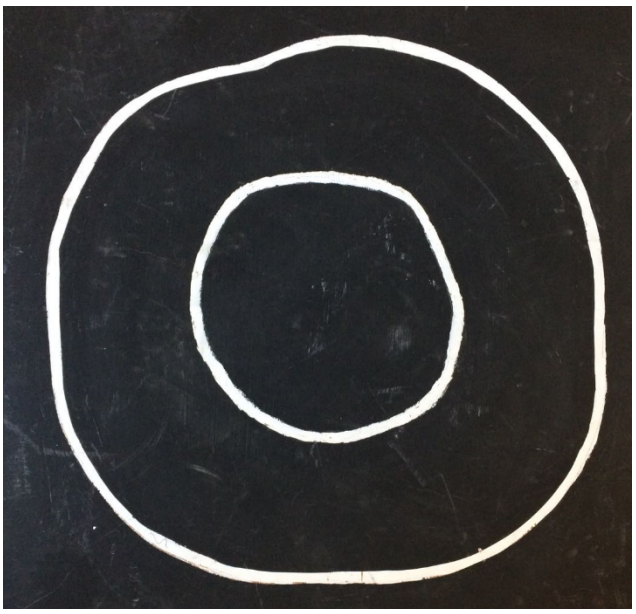

Figure 8. The motion line path of the robot

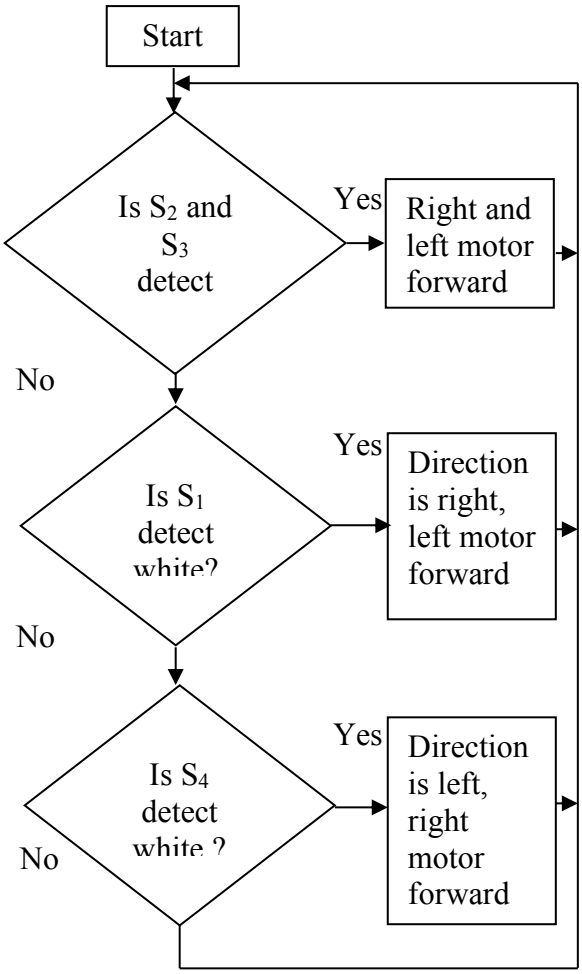

Figure 9. Line tracking algorithm

Fig.10 shows the block diagram of the battery-free robot system operating with wireless energy transfer. Amplitude modulation carrier signal frequency is 112 kHz. Magnetic field amplitude modulation shows simultaneous broadcast communication between surface and the robot.

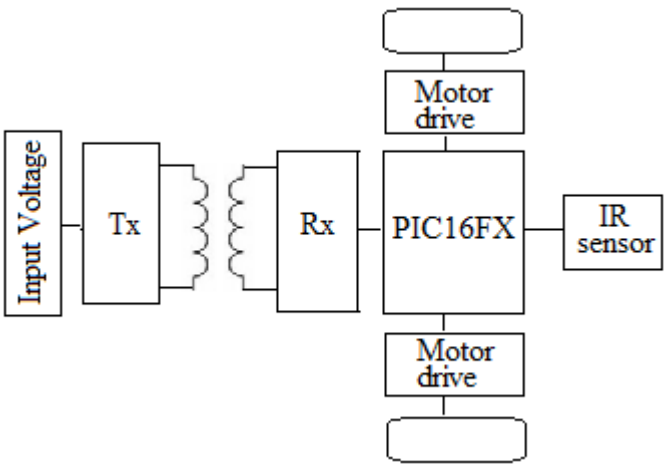

Figure 10. The block diagram of wireless robot system

3. CONCLUSION

The use of wireless energy transmission is increasing day by day. In this study, wireless power transfer was provided to mobile robots designed to operate with low power and without battery. The transmission of the electric energy simultaneously distributed to the robot moving surface to the robots without the conductive material and the battery has increased the robot mobility. At the same time, the elimination of battery costs and battery maintenance costs indicate that a low-cost and low-power mobile system in industrial transportation can be included in the production band. The fact that the work being done is microcontroller-based allows for the implementation and development of its decision-making mechanism without the need for a remote control.

REFERENCES

[1] Liu Z.T., Zhong Z., Guo Y.X., In vivo high-efficiency wireless power transfer with multisine excitation, IEEE T Microw Theory 2017; 65(9): 3530-3540.

[2] Imura T., Hori Y., Maximizing air gap and efficiency of magnetic resonant coupling for wireless power transfer using equivalent circuit and Neumann formula, IEEE T Ind Electron 2011; 58(10): 4746-4752.

[3] Lim J., Byunghun L., Maysam G., Optimal Design of a Resonance-Based Voltage Boosting Rectifier for Wireless Power Transmission, IEEE T Ind Electron 2018; 65(2): 1645-1654.

[4] Germano P., Perriard Y., Battery Charger for Electric Vehicles based on a Wireless Power Transmission, CES Transactions on Electrical Machines and Systems 2017; 1(1):66-71.

PERFORMANCE EVALUATION OF HARMONICS ON POWER QUALITY: CASE STUDY

Kaleid Waleed Abid[1], Younis Khalaf[2], Osama Ibrahim[3], Mohammad Safar[4], Saygin Siddiq Ahmed[5]

[1]Renewable Energy Research Center, University of Anbar, Iraq, kaleidwaleedabid@gmail.com

[2]University of Anbar, Renewable Energy Research Center, Iraq, younis_1976@yahoo.com

[3]Renewable Energy Research Center, University of Anbar, Iraq, osama_eng21@yahoo.com

[4]M.S.c. Research at Gaziantep University, mehmet.sefer.ms@gmail.com

[5]Ph.D. Research at Gaziantep University, saygin.basha@gmail.com

ABSTRACT: This work is proposed the results of current and voltage measurements in the real low voltage distribution system and explains the effects of Harmonics in the Power System with high accuracy with many factors, the relationship between the load and no load and its effects on electrical equipment are practically analyzed , caused by connecting the resistive load and no loading with conclusion two form frequencies, the system behavior is analyzed using the power quality analyzer device (Fluke-435B). This paper will imitate to these sets and include graphs which should explain the variances between individual power quality disturbances. the analysis of the results with respect to k factor and THD and how these can be analyzed to check more successfully w.r.t IEEE 519 are showed. The elements of the distribution system consist of:1 kVA transformer, load resister, and Adjustable Speed Drivers(ASJ) are modeled.

Keywords: Power System, Harmonics, THDi , THDv, Kfactor, Power quality, LVDS, RERC.

INTRODUCTION

The Harmonic disturbances were principally less in the earlier period as the designs of power systems were very easy and conformist. However, these days with using of compound devices in the industry and traditional harmonic disturbances has too enlarged. So the Harmonics are one of the highest worries in a power system investigates.

There are numerous resolves aimed at the standards which are taking from the power quality. One of the highest details is the consumers are well informed about

the power quality subjects like interruptions, sagging and switching transients. Besides, many power organizations are internally joined to low voltage network. The component of electrical power (current and voltage) distortion waveforms caused by harmonics are realizing to weaken of the power systems analyses [1,2].
The harmonics produce in a power system from two different forms of loads. The First type of loads is entitled the linear loads. The linear time-invariant loads are deliberated which the function of sinusoidal voltage outcomes in a sinusoidal drift of current. Aconstant steady-impedances are directed from these loads through the applied sinusoidal signals. The Non-linear loads are considered the second kind of loads. The application of sinusoidal voltage does not consequence in a sinusoidal flow smeared sinusoidal voltage for a non-linear devices.
The non-linear loads draft a current which may be discontinuous and distortion. The power system in the Iraq uses a fundamental frequency of 50 Hz. All loads are reproduction to receive untainted sinusoidal waveforms however due to non-linear loads, the untainted sinusoidal waveforms are distorted by electromagnetic phenomena called harmonics [3,4, 5]. Harmonics are contenting of the signal that frequency is an integer multiple of the system's fundamental frequency, Harmonics for this frequency are shown in Table 1.

Table 1: Fundamental frequency of 50 Hz and its harmonic values

Nth Harmonic	Fundamental	2nd Harmonic	3rd Harmonic
N(50) Hz	50 Hz	100 Hz	150 Hz

The other variables may be ducked as the dc presents a less angle pattern and the detailed analytical procedure is functional [6]-[8]. This detailed analytical procedure (DAPs) uses the Laplace transformation requires estimations of lengthy inverse Laplace transformations [6] or the state variable approach [7]. Once a study is complete, a report will be issued containing:

Voltage & current harmonic distortions
Graphical one-line display of harmonic results
Voltage & current harmonic spectrum plots
Updated one-line diagram (optional)
Fundamental load drifts outcomes
Recommendations for corrective action

This paper presents a measurement of the total harmonic distortion levels and k-factor created by ASD in building contents of twenty labs. materials, Refrigeration & Air Conditioning,electrical test, solar energy, electronic lighting ballasts, uninterruptible power supplies,Number of printers therefore, The effect of phase shift transformers and distortion are inspected and cast-off as methods to analyses the harmonic distortions.

POWER LOSSES

The Non-linear loads that cause harmonics are magnetic devices, converters, and rotating machines. Many motors that are used in industrial applications are collected of magnetic materials and are driven by a changing flux and magnetic field. This increasing a back electromotive force (EMF) and straight contributes to a form of harmonic distortion known as as voltage distortion. The harmonic currents are generated by non liner loads, additional losses in the transformers feeding the loads. The overall load loss be able to be listed as:[9]-[11].

$$R_{EC_R} = R_{AC_R} - R_{DC} \quad (1)$$

$$R_{EC_R} = R_{AC_R} - R_{DC} \quad (2)$$

$$P_{Load} = I2\,R_{DC} + P_{EC} + P_{OSL} \quad (3)$$

$$P_{Load} = I2\,R_{DC} + P_{EC} = I2_{RDC} + I2\,R_{EC} - R(f_h/f_L)2 \quad (4)$$

Table 2: Fundamental frequency of 50 Hz and its harmonic values

PLoad	The totalload of the transformer
I	the rms current
R_{DC}	Winding DC resistance
P_{DC}	the winding eddy-current loss
R_{EC-R}	is the equivalent resistance corresponding to the eddy-current loss
f_t	The Individual harmonic
f_L	The Fundamental frequency
POSL	POSL is the other stray loss

Small dc modules (up to the rms magnitude of the transformer excitation current at rated voltage) are predictable to have no effect on the load carrying capability of a transformer determined by this optional practice. Higher DC components may unfavorably affect transformer proficiency and should be avoided [12]-[14]. In observation, it is important to use the real harmonic current values sooner than theoretical values [15].

ESTIMATION OF HARMONIC LOAD METHODS

The IEEE Standard 1100-1999 distinct power quality disturbances based on the wave shape. There are five primary categories of waveform distortion:

1. DC offset
2. Harmonics
3. Inter harmonics
4. Notching
5. Noise

There are three methods for estimation harmonic load content:

Total Harmonic Distortion(THD)

Distortion Index, the best commonly used directory for computing the harmonic gratified of a waveform, is the total harmonic distortion (THD). It is a degree of the actual importance of a waveform and can be practical to both voltage or current. Just as waveforms can be added to generate imprecise signles, distorted components may be decomposed into fundamental and harmonic signles. This guide can be intended for either current and voltage. [8,9,16]. The following formulas are computing the total harmonic distortion for both 17

$$\%THDI = \frac{\sqrt{\sum_{h=2}^{h=\infty}(Ih)^2}}{I1} \quad (5)$$

$$THDi = \sqrt{(\frac{\text{Irms}}{\text{I1}})^2 - 1} \quad (6)$$

$$\%THDv = \frac{\sqrt{\sum_{h=2}^{h=\infty}(Vh)^2}}{V1} \quad (7)$$

$$THDv = \sqrt{(\frac{\text{Vrms}}{\text{V1}})^2 - 1} \quad (8)$$

K-Factor Rated Transformers

K-factor transformers are considered to stream non-sinusoidal loads, and there are used smaller, insulated, the secondary conductor in matching to reduce skin effect, but that is more expensive than conventional transformers[8,9,16].The zero sequence current goes in the neutral as the majority harmonic current frequencies comprise harmonic components consuming multiples of (3,6.9…etc.).

$$K = Pt/Pf = \sum_{h=1}^{h=\infty}(Ih)^2\, h^2 \quad (9)$$

Crest factor method

It is means of determining the max load that can be safely placed on a transformer which deliveries harmonic loads.By definition, a perfect sine wavecurrent or voltage will have a crest factor of 1.414, and any deviation fromthis value represents a distorted waveform[11,12,13].

$$CF = \frac{Peak\ Magnitude\ of\ current\ waveform}{True\ RMS\ of\ the\ current} \quad (10)$$

HARMONIC LIMITS (DISTORTION LIMITS)

Bear in mind that ahead of harmonics may still be necessary, whether or not the aim is to meet IEEE Std. 519-1992 standards. In low-voltage schemes (600 V or less), capacitors are generally the deepest impedance at harmonic frequencies, and practice as a result high RMS currents and enlarged the temperature that sources them to burn.

Harmonics Stander Limit

According to IEEE 519, harmonic voltage distortion on power systems 69 kV and below are restricted to 5.0% total harmonic distortion (THD) with each harmonic

restricted to 3%. The harmonic current limits vary based on the shortcircuit strength of the system they are being injected into basically, the new system can hold harmonic currents, The utility switches providing a clean voltage to the customer.

ISC/IL Ratio

As presented in Table 2 and stated previously in this work, the harmonic limits which apply to a particular customer depend on the ISC/IL ratio at that customer's point of common joining with the utility. As distincted in IEEE 519 ISC is the maximum short-circuit current at PCC. This should be a three-phase bolted fault current. This is a current calculated from the maximum billing (e.g. 15 or 30minute) demand, not an instantaneous peak—avery important distinction. This ratio indications the relative impact that a given customer can have the utility. Acustomer with a small demand relative to the short circuit current available cannot cause much disruption to the utility system. The actual measurement on non-linear devisees is very imported to devices specifications in zones and construction such that the maximum total harmonics distortions (THD) of circuit currents,at rated load conditions, shall be restricted to those figures as presented in Table 3 below.

Table 3. Maximum THD of current in percentage of fundamental

Circuit Current at Rated Load Condition 'I' at 380V/220V	Maximum Total Harmonic Distortion (THD) of Current
I<40A	20.0%
40A≤I<400A	15.0%
400A≤I<800A	12.0%
800A≤I<2000A	8.0%
I≥2000A	5.0%

The maximum acceptable of fifth harmonic current distortion (THDi5) at the Adjustable Speed Drives (ASD) operation within the variable speed range is less than 35%. The compensation group at sub-panel is accepted in this state [18].

EXPERIMENTAL SETUP

The experiments parts were performed on a single phase transformer. The results value is very accurate because All result parameters were got with theFluke-435B power quality analyzer. Open- Circuit and Short-Circuit tests were applied to a 1kVA, 220/105-V single-phase transformer.

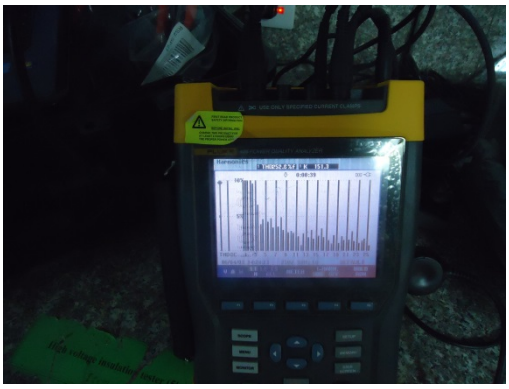

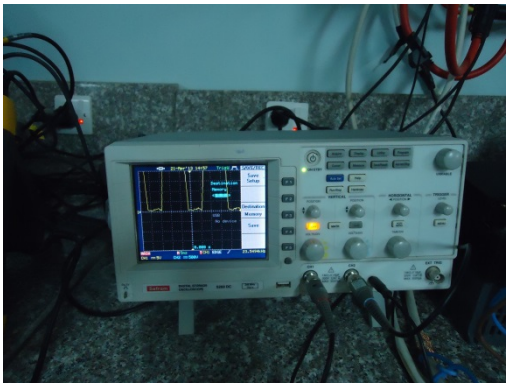


N700E
HYUNDAI

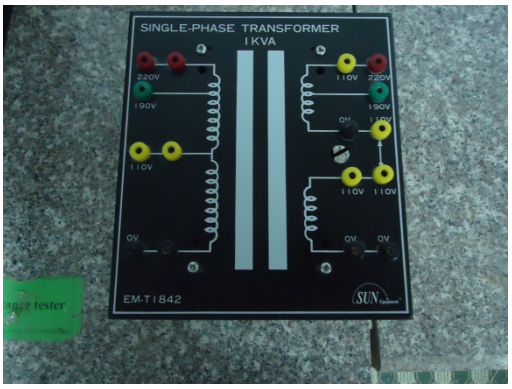
SINGLE-PHASE TRANSFORMER
1 KVA
220V
190V
110V
0V
EM-T1842
SUN

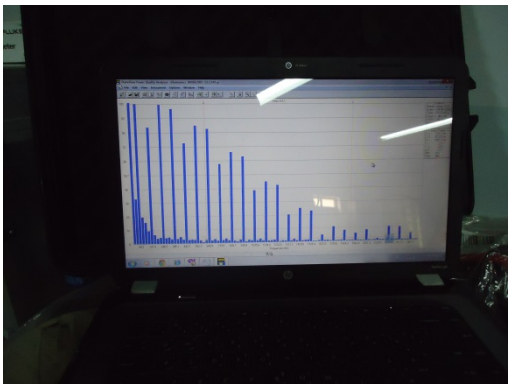

Table 4. List of used components in the experiment

item	Model number(specifications)
ASD	N700E
Power quality analyzer	Fluke-435B
Many Variable resistors	From 500w to 1000w
435BStorage oscilloscope	SFRAM
Transformer	1KVA
Personal Computer	

Figure 1. Practical experimental components Harmonics Effect at Frequencies.

RESULTS and DISCUSSION

Using mat lab Program, the values of internal resistance is showed for different frequencies, according to noload and load at Fig(2) and Fig(3), without DC effects, the normalize of the first one is 0. 1263 and the second one is 0. 1466 for 16 points used for fitting for each other at 50 Hz.

The Total Harmonic Distortion (THD) Using power quality analyzer, is computed at the PCC and (fig.6 to fig.11) show that. Results are presented in approximate percentage of the 50 Hz component. The current flow in the neutral is distorted with following percentage, At no load case the THDi and k factor 57.4%,14.6 respectively. However, at load THD and k factor 64.9%,19.4 respectively. The increasing value of Thai and k factor is 11.55%,24.74 respectively.

The current flow in the line is distorted with following percentage, At no load case the Thai and k factor 77.6%,81.3 respectively. Though, at load THD and k factor 230.1%, 178.3 respectively. The increasing value of Thai and k factor is 66.27%,54.4 respectively.

The voltage distortion in the neutral is distorted with following percentage, At no load case the THDv =67.9%. But at load THDv = 88.6 %,. The increasing value of THDv is23.36%, the Total Harmonic Distortion (THD) is computed at the PCC For 50 Hz show that.

At 400 Hz, (fig.12 to fig.17)The current flow in the neutral is disfigured with following percentage. At no load case the THDi and k factor 68 %, 21 respectively. However, at load THD and k factor 108.6%, 36.3 respectively. The increasing value of THDi and k factor is 37.3% 42.2 respectively.

The current flow in the line is distorted with following percentage. At no load case the THDi and k factor 226.6% 169.8 respectively. However, at load THD and k factor 182%, 93 respectively. The increasing value of THDi and k factor is (- 24.5 %,-82.5) respectively. The voltage distortion in the neutral is distorted with following percentage. At no load case the THDv = 90.8%. But at load THDv = 38.3 % The increasing value of THDv is (- 1.37 %).

Table 5. Parameters Analysis under states of variable Load Conditions

		April(A)	Armsl(A)	Arms 9N(A)	ApkN(A)	Vrms (V)	Vpk (V)	THDil	K factor	CFLv
At 50hZ no load	Resistive load	11	2	2	4	227.52	317.5	77.6	81.3	1.40
At 50 hz load		11	2	2	4	225.69	316.2	230.1	178.3	1.4
At 400hz no load		6	1	1	2	229	326	226.6	169.8	1.41
At 400 hz with load		13	4	1	4	220	310	182	93.7	1.42

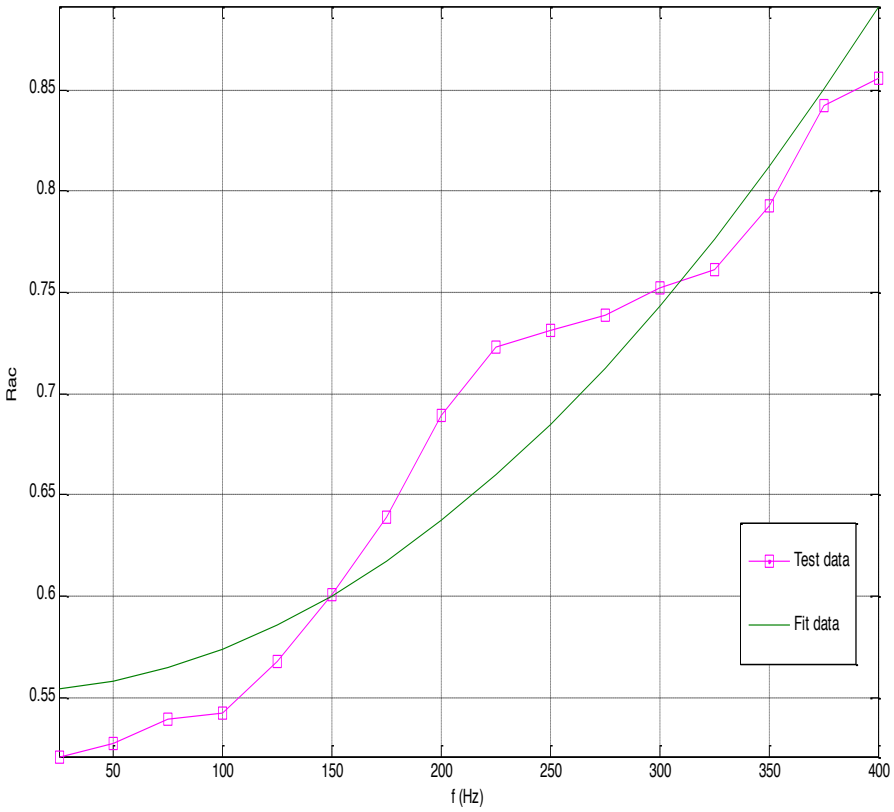

Figure 2. At no load

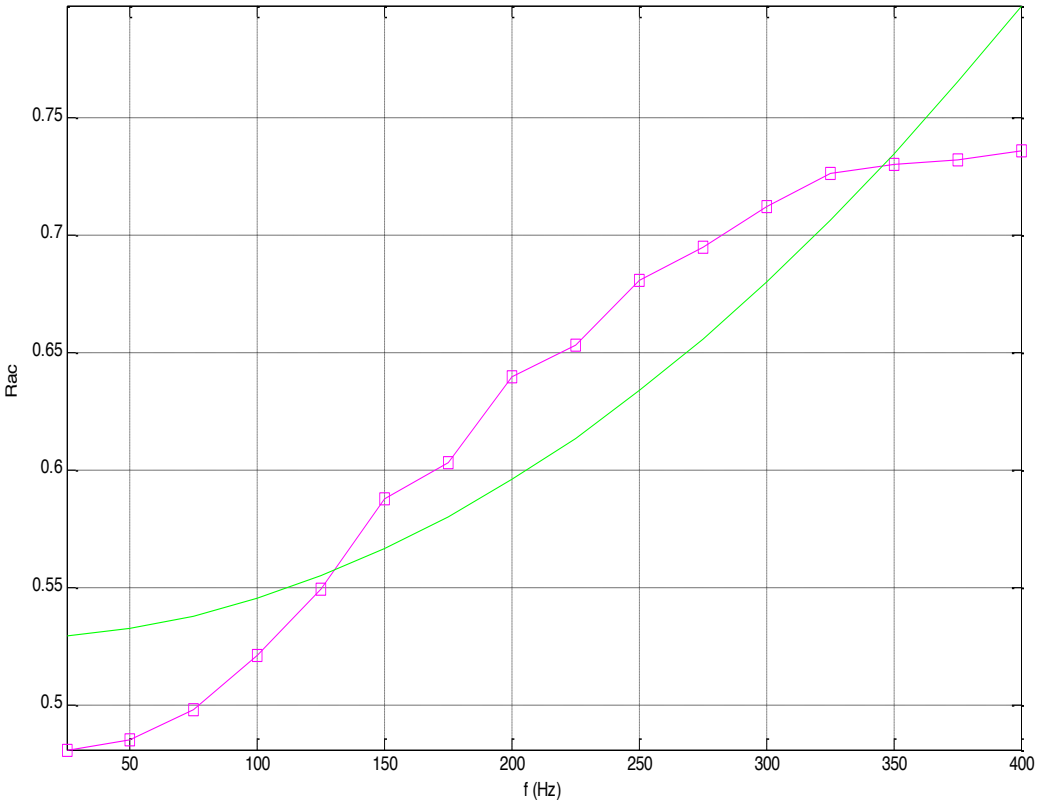

Figure 3. At load

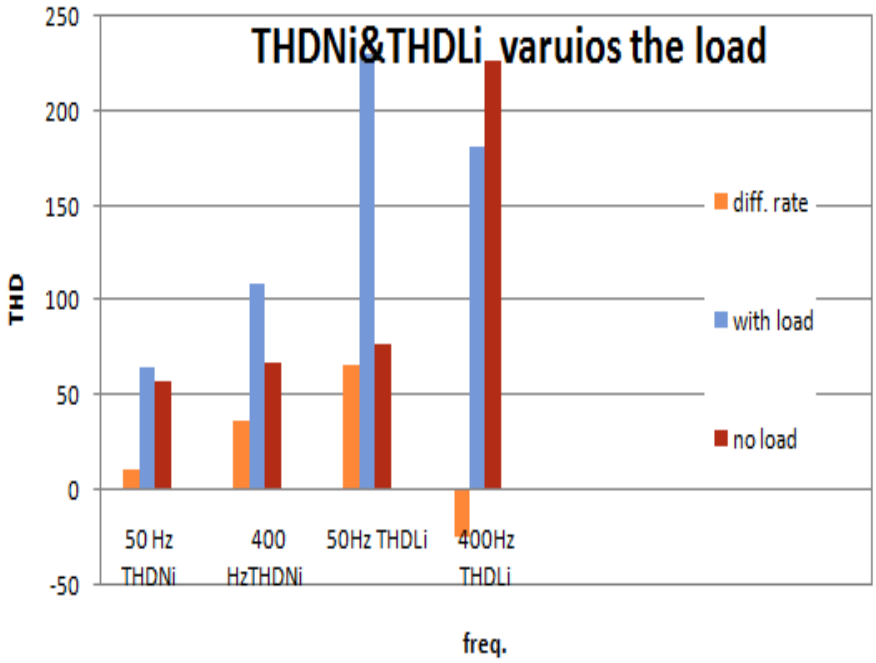

Figure 4. Amplitude of THDNi and THDLi at (50Hz and 400Hz) with and without resistive load (neutral and line for the current waveform)

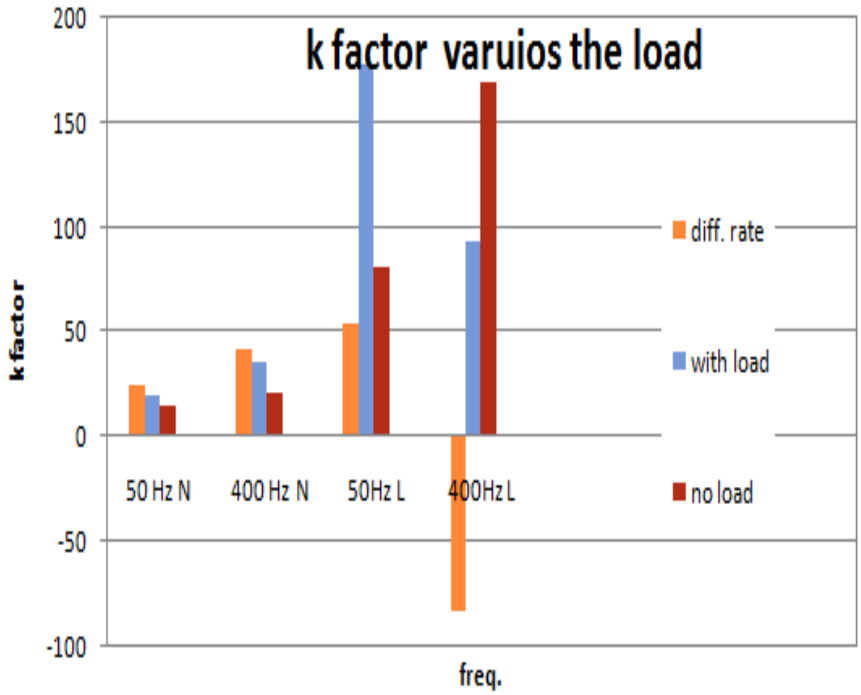

Figure 5. Amplitude of the k factor at (50Hz and 400Hz) with and without resistive load (neutral and line for the current waveform)

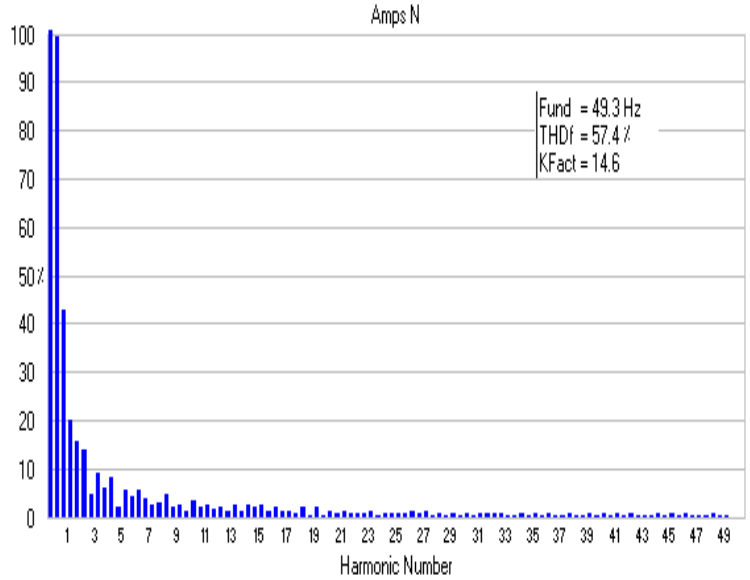

Figure 6. Amplitude of Harmonics at 50Hz without resistive load (neutral line for the current waveform)

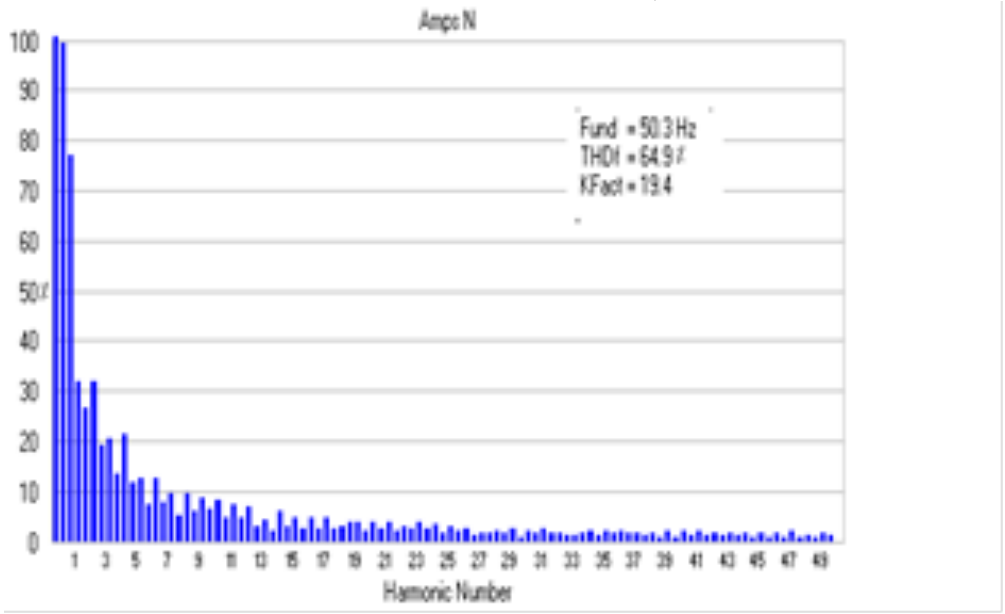

Figure 7. Amplitude of Harmonics at 50Hz with resistive load (neutral line for the current waveform)

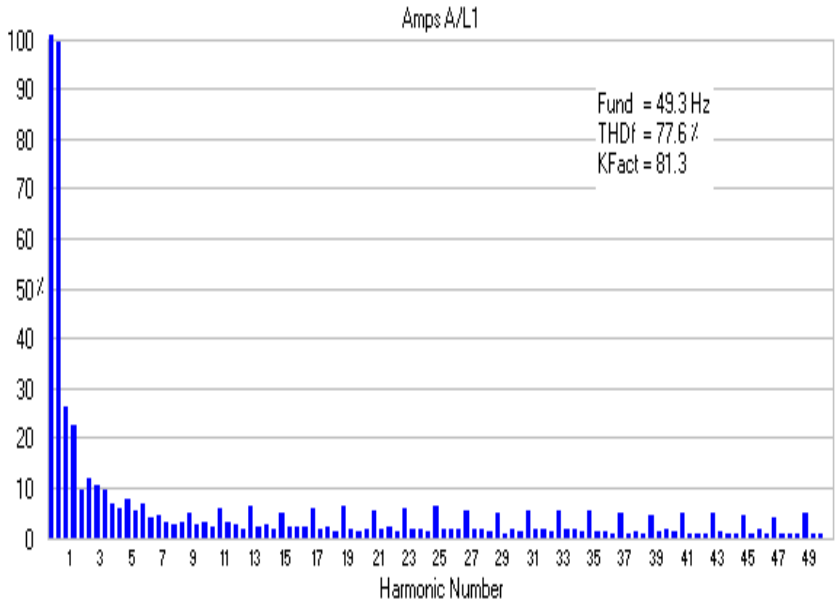

Figure 8. Amplitude of Harmonics at 50Hz without resistive load ((Line harmonics for the current waveform)

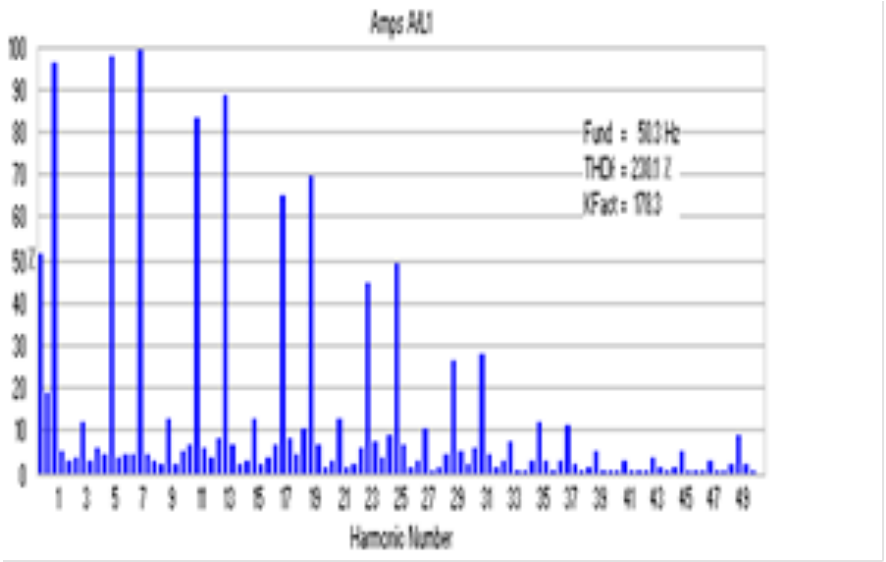

Figure 9. Amplitude of Harmonics at 50Hz with resistive load ((Line harmonics for the current waveform)

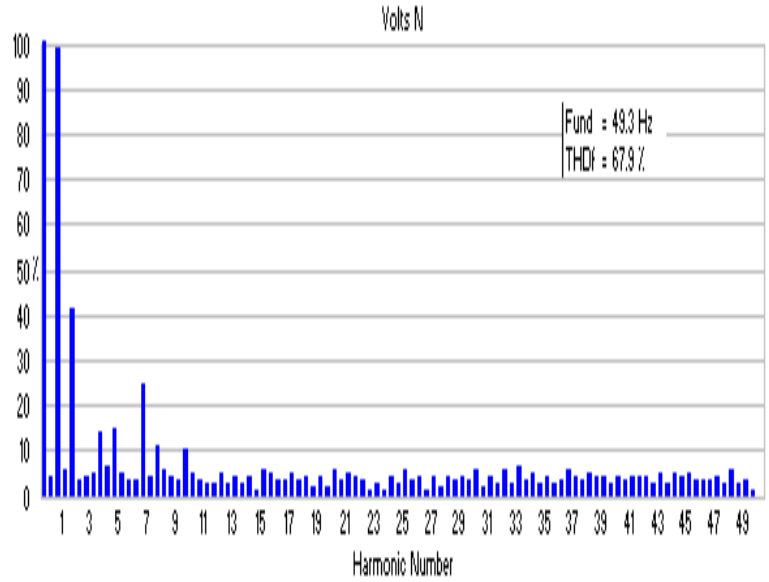

Figure 10. Amplitude of Harmonics at 50Hz without resistive load (Neutral Line harmonics, volt)

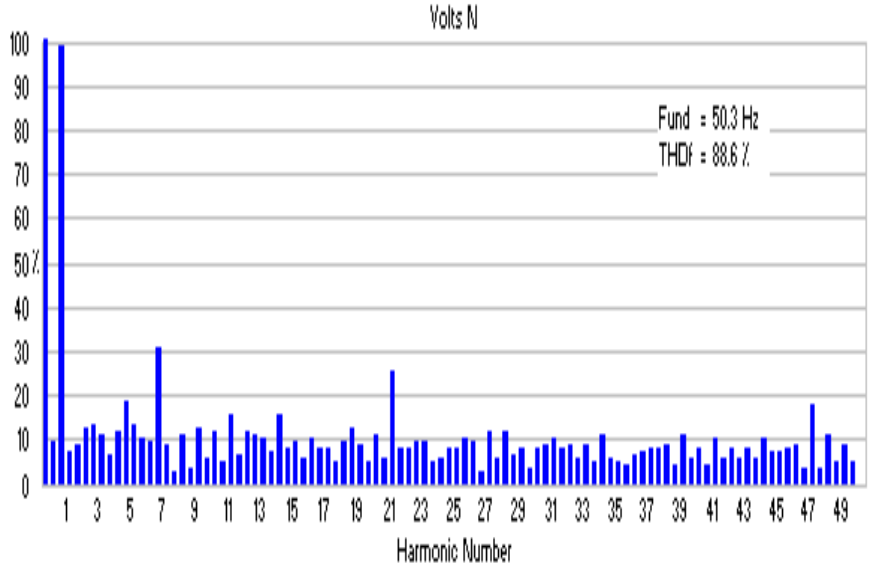

Figure 11. Amplitude of Harmonics at 50Hz with resistive load (Neutral Line harmonics, volt)

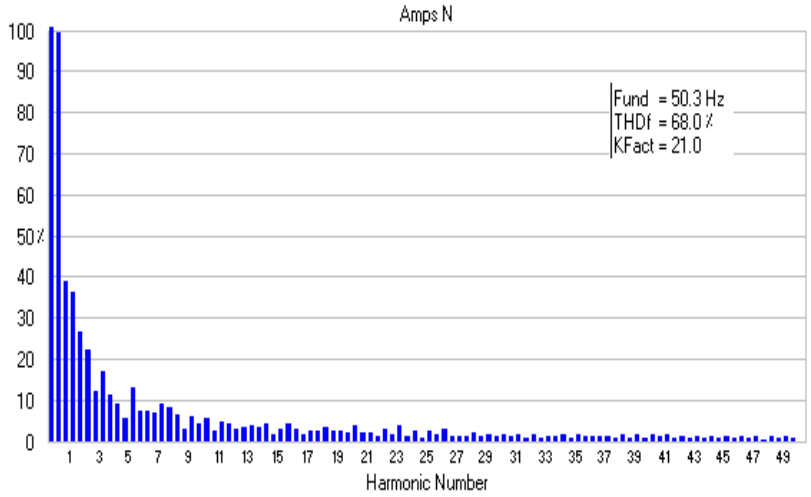

Figure 12. Amplitude of Harmonics at 400Hz without resistive load (neutral line for the current waveform)

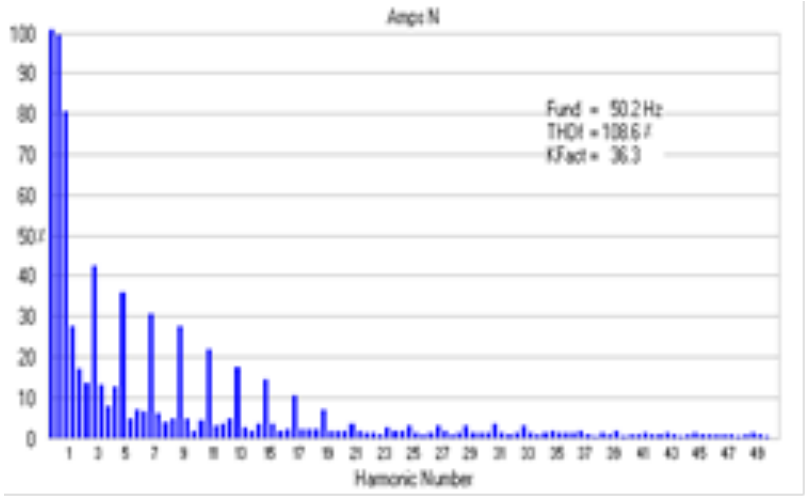

Figure 13. Amplitude of Harmonics at 400Hz with resistive load (neutral line for the current waveform)

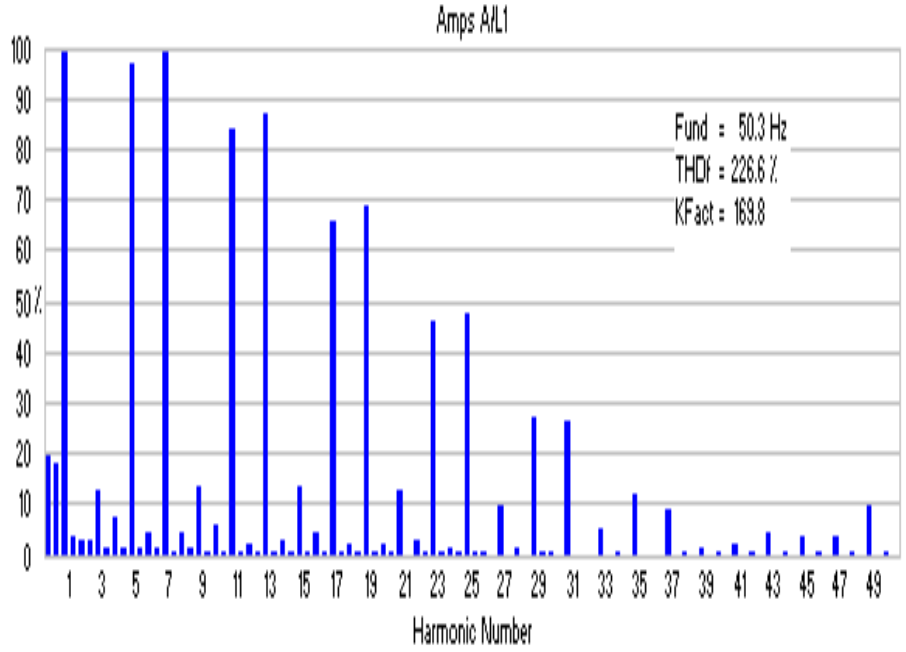

Figure 14. Amplitude of Harmonics at 400Hz without resistive load (Line harmonics for the current waveform)

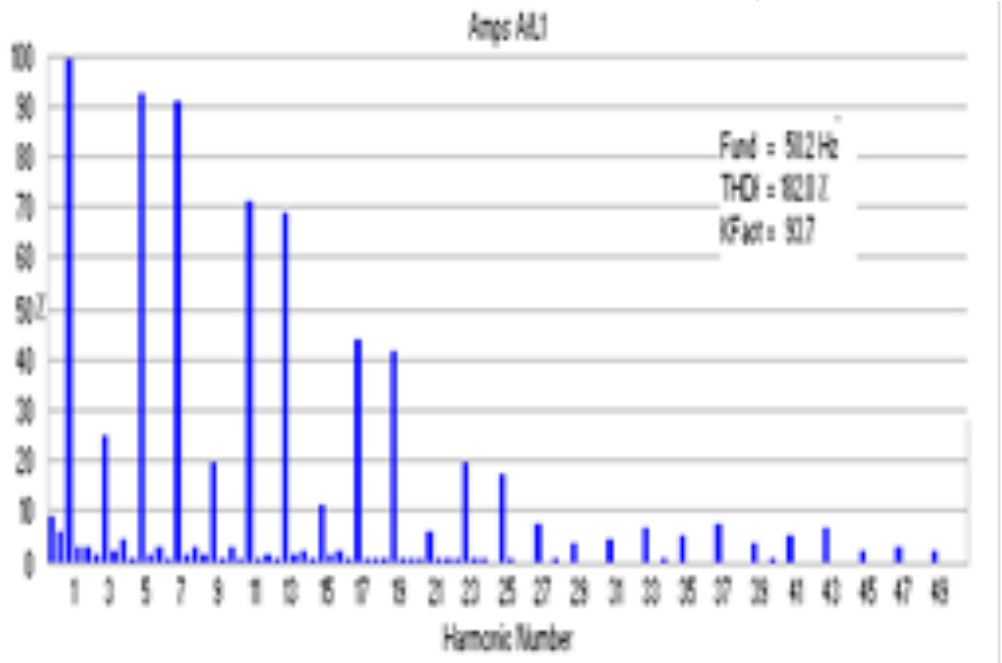

Figure 15. Amplitude of Harmonics at 400Hz with resistive load (Line harmonics for the current waveform)

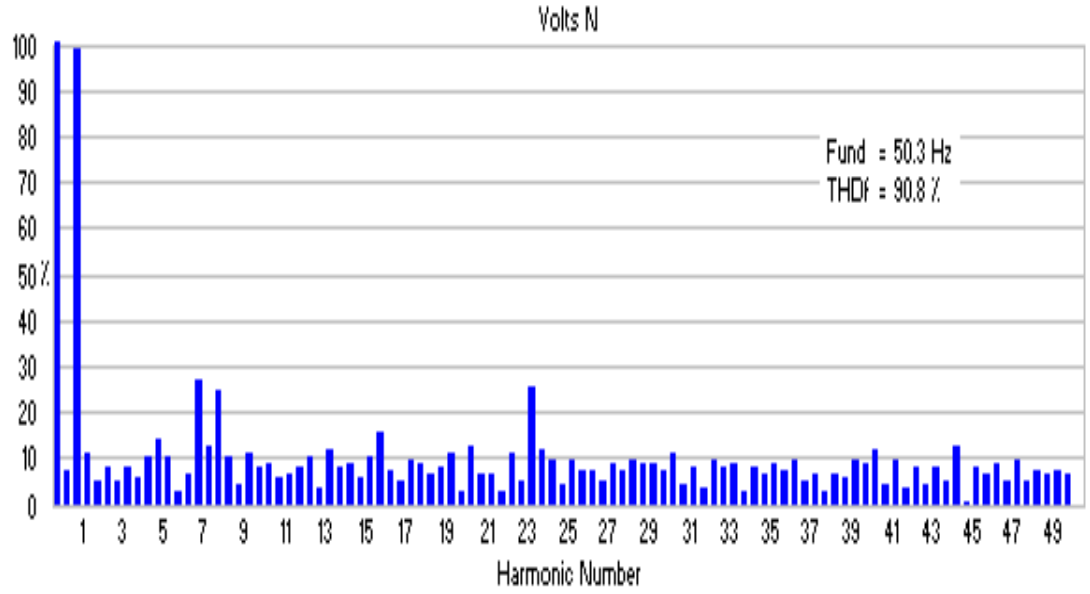

Figure 16. Amplitude of Harmonics at 400Hz without resistive load (Neutral Line harmonics, volt)

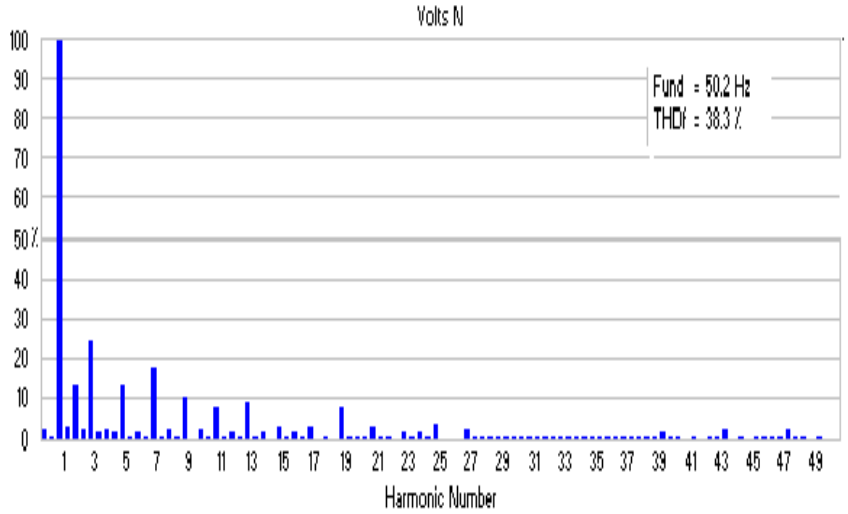

Figure 17. Amplitude of Harmonics at 400Hz with resistive load (Neutral Line harmonics, volt)

CONCLUSIONS

In this investigation two kinds of frequency, the first50 Hz and the second 400Hz under no load and pure resistive load. At no load and load Have been observed of THDNi increasing with frequency,the values w.r.t the line distortion it low because overlap waveform,the phase shift between the phases decreases, PCC and flow direction of all harmonics. The behavior at no load and load of THDLi is changed at 400 Hz only where the value of THDLi at no load higher than load because changed the electrical load of building. The behavior of the THD is the same behavior of K-factor However, this values exceed over the rate of IEEE 519(I<40A) cause by their many technical labs, in this building of RERC. Both No load and Load losses are effected by the presence of harmonics in load currents.

However, the variation in load losses contributes more to excessive heat generation in distribution transformer. The Fluctuation between the high and the low-frequency especially at increasing the load is present this must take into consideration when designing and manufacture of Electric devices.

RECOMMENDATIONS FOR FUTURE WORK

New laboratory tests on dissimilar transformers are required. A wide study of loads such as the individually of the inductance or capacitance is required for finally this issue. To rise above this state the optional action is to twice over the size of the neutral.

ACKNOWLEDGMENTS

This work is supported by the University of Anbar-Iraq/Renewable Energy Research Center with Grant No. RERC-PP36.

REFERENCES

Yu, Y., Liu, K., Fu, B., & Zhao, Y. (2009). Harmonic and interharmonic currents generated by the VSI-fed adjustable speed drive. 2009 IEEE 6th International Power Electronics and Motion Control Conference. doi:10.1109/ipemc.2009.5157817.

IEEE Recommended Practices and Requirements for Harmonic Control in Electrical Power Systems. (n.d.). doi:10.1109/ieeestd.1993.114370.

Salih Mohammed Salih, Kaleid Waleed Abid and Munther Nayef, "Practical Analysis of Harmonics Effects on Transformer", Renewable Energy Engineering, 70, 24362-24367, 2014.

IEC 61000-3-6 Edition 2.0 2008-02, Electromagneticcompatibility (EMC) – Part 3-6: Limits – Assessment of emission limits for the connection of distortinginstallations to MV, HV and EHV power systems, Geneva, Switzerland,2008.

Hoevenaars, A. H., Evans, I. C., & Lawton, A. (2008). Meeting new marine harmonic standards. 2008 55th IEEE Petroleum and Chemical Industry Technical Conference. doi:10.1109/pcicon.2008.4663983.

G. Carpinelli, F. Iacovone, A. Russo, P. Varilone, and P. Verde,(Jul.2004)"Analytical modeling for harmonic analysis of line current of VCI-feddrives," IEEE Trans. Power Del., vol. 19, no. 3, 1212–1224.

K. L. Lian, B. K. Perkins, and P. W. Lehn, (Apr. 2008.) “Harmonic analysis of athree-phase diode bridge rectifier based on sampled-data model,” IEEE Trans. Power Del., vol. 23, no. 2, pp. 1088–1096.

Julio G. Mayordomo, Member, IEEE, Luis F. Beites, Ángel Carbonero, Xavier Yang, Senior Member, IEEE,and Wilsun Xu, Fellow, IEEE (2015)“An Analytical Procedure for Calculating Harmonics of Three-Phase Uncontrolled Rectifiers Under Non ideal Conditions” IEEE Transactions on Power Delivery, ISSN 0885-8977.

JianZheng (2000) "Transformer ac winding resistance and derating when supplying harmonic-rich current" "M.Sc. A thesis in electrical engineering in Michigan Technological University".

ABS (2006) Guidance Notes on Control of Harmonics in Electrical Power Systems, "American Bureau ofShipping".

H. García, M. Madrigal, J.J. Rico,(2012) " The use of companionharmonic circuit models for transient analysis and periodicsteady state initialization in electrical networks withnonlinearities", Electric Power Systems Research, volume 93, 46–53.

Task Force on Harmonics Modeling and Simulation,(2004) “Modeling devices with nonlinear voltage-current characteristics for harmonic studies”, IEEE Transactions on Power Delivery, Vol. 19, pp. 1802-1811.

K.C. Umeh, A. Mohamed, R. Mohamed,(2003) “Determining harmonic characteristics of typical single phase non-linear loads”, Proc. Student Conference on Research and Development (SCORED), Putrajaya, Malaysia.

Task Force on Harmonics Modeling and Simulation,(2004) “Modeling devices with nonlinear voltage-current haracteristics for harmonic studies”, IEEE Transactions on Power Delivery, Vol. 19, 1802-1811.

Dr. Abla GADO, Eng. Hassan ABO GAD, Eng. Salah RADWAN (2011) “EFFECT OF TYPES OF LOADS IN RATING OF TRANSFORMERS SUPPLYING HARMONIC-RICH LOADS”, 21st International Conference on Electricity Distribution Frankfurt.

Jonathan Blackledge, Eugene Coyle and Kevin O’Connell (2013),“Proximity Heating Effects in Power Cables”, Dublin Institute of Technology, IAENG Letters, forthcoming.
Dugan RC,(1994) "Electrical Power Systems Quality" McGraw Hill Companies.

Ir. Martin WU Kwok-tin,(2003) “Standards of Power Quality with reference to the Code of Practice for Energy Efficiency of Electrical Installations”, Energy Efficiency Office, Electrical & Mechanical Services Department.

Ahd H. Gheeth (2012)"Analysis Of Power Transformers Feeding Variable Frequency".